FATIGUE LIFE ASSESSMENT OF 5 MW ONSHORE WIND TURBINES

by

Onur Kalan

B. S., Civil Engineering, Boğaziçi University, 2010

Submitted to Institute for Graduate Studies in
Science and Engineering in partial fulfillment of
the requirements for the degree of
Master of Science

Graduate Program in Civil Engineering

Boğaziçi University

2012

ACKNOWLEDGEMENTS

I would like to express my gratitude to my thesis supervisor, Assist. Prof. Serdar Soyöz for his valuable guidance, support and help in every stage of this project. It was a great pleasure for me to work with him.

I also would like to thank to Assoc. Prof. Hilmi Luş and Assist. Prof. Can Aydıner for their knowledgeable and in-depth comments and advices.

I would like to extend my thanks to my dear friend Melik Ertuğrul for being helpful and his friendship. I wish you success, luck and happiness.

Finally, I would like to express my gratitude and respect to my family Nurdoğan Kalan, Semran Kalan, Özgür Kalan, Barış Kalan for their encouragement, continous support throughout my life.

ABSTRACT

FATIGUE LIFE ASSESSMENT OF 5 MW ONSHORE WIND TURBINES

Renewable energy is a significant part of energy sector due to its economical and natural reasons. The modern wind turbines can be designed such that they are resistant to the heavy loads and and excessive forces because of the technological improvements. On the other hand, these type of systems should be durable against other design parameters such as fatigue. In this study, a 5 MW onshore wind turbine was analyzed against fatigue failure at the bolted joints. Initially, soil uncertainty is investigated in terms of soil stiffness that is represented by subgrade reaction of modulus. Change in soil stiffness due to soil uncertainty leads to change in overall period of the structural system. This situation may result in resonance and; therefore, the fatigue life of the structural parts changes significantly. A 5 MW onshore wind turbine model is created in the FAST (Fatigue, Aerodynamics, Structures and Turbulence) program which is a tool that can perform dynamic analyses for wind turbines under stochastic wind loading. Effect of resonance is investigated in terms of base shear and over-turning moment obtained from FAST analysis. Two different cases; namely, ”in-resonance” and “out-of-resonance” cases have been considered to compare the fatigue life of the structural parts. It was found that the fatigue life of the “in-resonance” case is decreased approximately to one third of the fatigue life of the “out-of-resonance” case. This observation reveals the importance of accurate modelling of the overall i.e. soil-foundation-structure system to obtain the actual structural period.

ÖZET

5 MW KARASAL RÜZGAR TÜRBİNLERİNİN YORULMA ÖMRÜ DEĞERLENDİRMESİ

Yenilenebilir enerji, ekonomik ve doğal sebeplerden dolayı enerji sektörünün önemli bir parçasıdır. Modern rüzgar türbinleri, teknolojik gelişmeler sayesinde, ağır yüklere ve büyük kuvvetlere karşı dayanıklı olarak tasarlanabilmektedir. Diğer yandan, bu tip sistemlerin yorulma gibi diğer tasarım parametrelerine karşı da dayanıklı olması gereklidir. Bu çalışmada, 5 MW'lık karasal rüzgar türbininin cıvatalı bağlantı parçalarında yorulma kırılmasına karşı analizi yapılmıştır. Öncelikle, zemin belirsizliği, yatak katsayısı ile temsil edilen zemin rijitliği açısından irdelenmiştir. Zemin belirsizliğinden kaynaklanan zemin rijitliğindeki değişim yapısal sistemin genel periyodunun değişmesine yol açmaktadır. Bu durum sistemin rezonansa girmesine neden olabilir ve bu sebeple, yapısal elemanların yorulma ömrünün önemli ölçüde değişmesine yol açabilir. 5 MW'lık karasal rüzgar türbin modeli, FAST (Yorulma, Aerodinamik, Yapılar ve Türbülans) isimli stokastik rüzgar yükleri altında dinamik analizler yapabilen program ile oluşturulmuştur. Rezonans etkisi, FAST analizinden elde edilen taban kesme kuvveti ve devrilme momenti açısından irdelenmiştir. Yapısal parçaların yorulma ömürleri kıyaslanırken "rezonans-içi" durumu ve "rezonans-dışı" durum dikkate alınmıştır. Şu sonuca varılmıştır ki; rezonans durumu esnasındaki yorulma ömrü, rezonans öncesi durumdakinin yaklaşık üçte birine inmektedir. Bu gözlem, gerçek yapısal periyodun elde edilmesinde bütün sistemin doğru modellenmesinin önemini açıkça ortaya koymaktadır.

TABLE OF CONTENTS

LIST OF FIGURES

LIST OF TABLES

LIST OF SYMBOLS

A	Area of the section, m^2
A_{rotor}	area of the rotor disk, m^2.
B	length of the footing, m
C	failure capacity
$C_D(\alpha)$	aerodynamic drag coefficient
$C_L(\alpha)$	aerodynamic lift coefficient
C_s	aerodynamic coefficient
c_α	airfoil chord length, m
D	outside diameter, m
E	Young's Modulus of elasticity, MPa
f	excitation frequency, Hz
F_D	aerodynamic drag force, N
F_L	aerodynamic lift force, N
f_n	natural frequency of the structure, Hz
F_{wind}	wind load, N.
F_y	yield strength, MPa
I	Area moment of inertia of the section, m^4
K	effective length factor
k	modulus of subgrade reaction, kN/m^3
k_B	appropriate subgrade reaction value, kN/m^3
k_{30}	subgrade reaction value obtained from Boussinessq Theory, kN/m^3
L	length of the foundation, m
l	unbraced length, m
M	Moment about the x-axis, kN.m
m_v	coefficient of volume compressibility, m^2/kN
N	Axial load, kN
N_i	cycle capacity of the material in i^{th} stress range
n_i	actual cycles in i^{th} stress range
p	net pressure per unit area of the foundation, m^2
q_0	net pressure on the foundation area, kN/m^2
r	radius of gyration, m
S_{oed}	settlement value, m

T	wall thickness, m
t	wall thickness, m
V_{disk}	wind velocity at airfoil, m/s
V_{rel}	relative wind speed at a blade section, m/s
V_{rot}	linear rotation speed at a blade section, m/s
V_{rotor}	wind velocity at the rotor, m/s
V_{tr}	transverse shear force, MN
V_0	wind velocity, m/s
y	location of the calculated stress point, m
Z	depth of the soil layer, m
α	angle of attack, deg
α	induction factor
ΔH	thickness of the compressible layer, m
Δq	average stress increment in compressible layer, kN/m^2
Δ_r	radial length of blade element, m
$\Delta\sigma$	average stress increment at the layer, kN/m^2
Θ	pitch angle, deg
λ	failure rate
μ	mean or expectation (location of the peak)
ρ_{air}	air density, kg/m^3
σ	standard deviation
Ø	angle of inflow, deg.
Ω	angular rotational speed, rad/s

LIST OF ACRONYMS/ABBREVIATIONS

API	American Petroleum Institute
BEM	Blade element momentum
BS	Base Shear
DAF	Dynamic amplification factor
EMRA	Energy Market Regulatory Authority
FAST	Fatigue, Aerodynamics, Structures, and Turbulence
GWEC	Global Wind Energy Council
NREL	National Renewable Energy Laboratory
OTM	Over-turning Moment
SAP	Structural Analysis Program
SDOF	Single degree of freedom
TurbSim	Turbulence Simulator
USD	United States Dollar

1. INTRODUCTION

Renewable energy has been one of the outstanding part of energy sector for a long time because this type of energy is relatively inexpensive and environmentally friendly. Wind energy is serviceable and continuous; that's why wind energy has become one of the most popular forms of renewable energy that has a share as of 2.67% in this industry. Especially in Turkey, onshore wind energy is making process each passing day.

Since wind turbine technology is improving day by day, more productive, more economic turbines with higher ultimate strength can be designed. These new generation wind turbines are resistant to certain types of heavy loads such as hub system loads and wind forces; however, these systems should also be checked against fatigue failure.

Onshore wind turbines are tall structures that contain heavy mass at the top of the tower. Additionally, they are prone to continuous wind forces that are time varying loads. Therefore, these structures are consistently subjected to the risk of resonance. In the case of resonance, especially joints in the structure can fail due to high cyclic loading in a time period that is shorter than expected. As a result, these critical joints should be analyzed in the design process by considering their fatigue life i.e. operational life.

A mat foundation with the dimensions of 15x15x3m is chosen as a support structure. This foundation is supported vertically and laterally by elastic springs to represent soil. A parametric study for the foundation stiffness is carried out by changing the subgrade reaction values, and the corresponding variation in the natural frequency of the system is observed.

1.1. Literature Review

In the literature, there are numerous studies about the wind turbine design concepts. First of all, the foundation modelling concepts for onshore wind turbines are summarized.

The foundation modelling of the onshore wind turbine is a significant part of the design process. Due to soil properties and uncertainties, the natural frequency of the

system differs significantly. There are several studies about foundation and soil modelling concept.

In a study by M.B. Zaaijer, different assumptions for the base support types of the wind turbine towers are introduced and the results are discussed. The relative importance of the various types of the foundation models is detailed as it can be seen in Figure 1.1 [1].

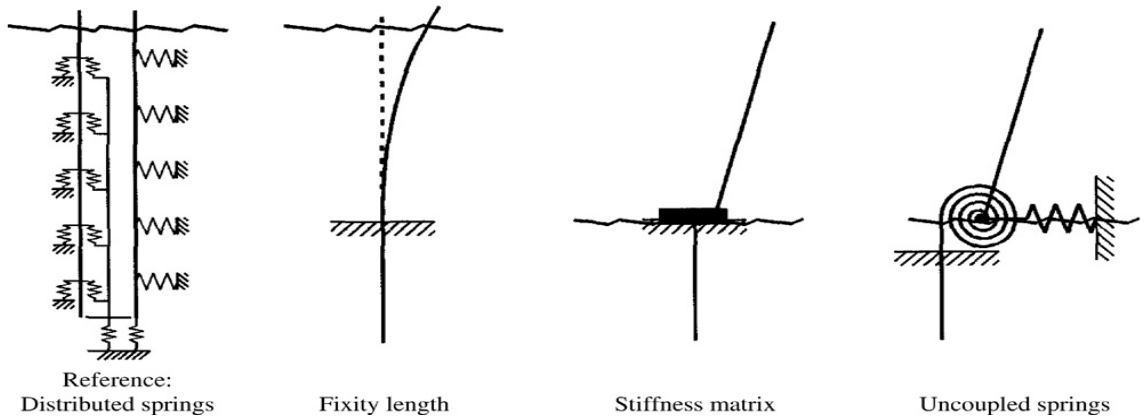

Figure 1.1. Different types of base supports [1].

The effective fixity approach is a reasonable approach especially for the tubular towers; however, the effective fixity length shows a large variation as a function of soil conditions. In Randolph's linear elastic model, the assumption is that piles longer than a critical length have the same behaviour as infinitely long piles; however, the pile length below the critical length and increased flexibility cannot be reached by Randolph's model. Reduced degree of freedom approach is a simplified method which is made by fixing some degrees of freedom; however, this approach does not meet the boundary conditions of the mode shapes in some models due to the extra constraints. The Finite Element Method based on the stiffness matrix approach gives good matches according to the expectations. Although small differences may occur due to the non-linear soil-structure interaction, this method gives sufficient results [1].

According to M. Kühn's study [2], choice of design properties of wind turbine's dynamic properties is very significant for an economical and reliable design solution. Aerodynamic loading, the interaction between sub-systems (e.g support structure-soil and

rotor-support structure) and cost efficiency are taken into consideration. In this study, “soft” or “stiff” foundation designs are mentioned. Foundation can be soft or stiff by increasing or decreasing the subgrade reaction of the soil. This behaviour causes the natural frequency of the system to differ.

Due to mass production, weight reduction and plant capacity, the wind turbine design has been getting more feasible. Two latter aspects have led designers to the “soft design” phenomenon for the hub systems and tower. Design concept can be chosen as “soft-stiff” or “stiff-stiff”, which means a soft tower with a stiff foundation or stiff for all. Furthermore, a well-designed system gains benefits in terms of dynamic response.

In several investigations about stiff-stiff and soft-stiff systems, blade excitation is beyond the natural frequency of the soft-stiff system and it leads to a lower dynamic amplification (DAF) than a stiff-stiff design [2].

A gradual decrease in stiffness from the foundation along the tower top gives more successful results in aerodynamic behaviour in terms of structural efficiency. Stiff-stiff characteristics are difficult to handle because of wind-induced fatigue. Hence, at least, the upper part of the system should be designed in such a way that it is flexible. However, the soft-stiff support structure concept is convenient for many sites but it is not possible for all generic concepts. It may be problematic if the design range for the fundamental natural frequency is not large or if the overall height of the tower is not sufficient for the design concept [2].

In S. Bhattacharya and S. Adhikari’s study [3], the estimation of the natural frequency of a wind turbine system with a surrounding soil is taken into consideration. In this paper, a single monopile is extended under the tower. The main objectives are to develop some testing methods for vibration analysis in different soil types, to validate the analytical approach and compare them with each other. It is concluded that the theoretical values show much higher values than the experimental values. The study shows that frequency is strongly related to the stiffness of the foundation. Generally, it is observed that analytical methods and finite element solutions overestimate the natural frequency [3].

In AlHamaydeh M. and S. Hussain's study [4], a frequency based foundation design is conducted for different wind turbines. The main idea is to observe the variations in the frequency of the system according to their foundation designs. In that study, multiple wind towers are located in different villages in Alaska. The towers are supported by two types of foundations: large mat and deep pile foundations. The installation cost, natural frequency and structural stability concepts are considered.

In the same study, idealized fixed base assumptions are made. However, assumption of fixed base design leads to overestimation of the system stiffness and under-designed systems may be built. Therefore, it is concluded that soil-structure interaction should be considered to get more realistic results [4].

In the design phase, the appropriate foundation type (spread footing, deep piles, etc.) with adequate stiffness is chosen to optimize the system natural frequency within the practical limits [4].

Figure 1.2. Reinforced Concrete foundation [4].

The foundation design is controlled by the natural frequency of structure-foundation system rather than by serviceability and strength. As a result, considering soil-structure interaction leads to obtaining more realistic estimation of the natural frequency [4].

In Y.I. Özdemir's study [5], the thick plates that rest on elastic foundations are investigated. In this study, analysis of isotropic plates on a Winkler foundation is considered. The concept of plates resting on elastic foundations is popular in structural engineering, especially for storage tanks, raft foundations, swimming pools, and so on [5]. In this thesis, the foundation model is similar to the elastic foundation described in the Y.I.

Özdemir's study. Winkler foundation approach is used to generate the appropriate subgrade modulus values in the foundation.

In another study about foundation modelling, the finite strip method is used. In this study, a thin plate and a Winkler elastic foundation are taken into consideration. Numerical results show that the spring system successfully simulates the different kinds of elastic supports [6].

Ayse T. Daloglu and C. V. Girijia Vallabhan's study [7] investigates the behaviour of soil on a Winkler foundation which is constructed by means of springs that are positioned underneath the structure. Those springs have their individually owned constants called "the modulus of subgrade reaction".

Generally, soil types are stratified with different thicknesses and different k values at each layer. The soil should have at least a thickness function for each soil layer. Thus, the whole soil system requires mathematical analysis to determine the settlements [7]. As a result, if a constant k value is used for uniformly distributed loads, the displacements are uniform and there are no bending moments or shear forces in the slab. To get more realistic values, higher k values should be placed at the edges of the slab [7].

In the onshore wind turbine design, the geometrical properties of the wind turbine have great importance as well as the foundation modelling. In this part, the geometrical effects of the wind turbine are described. Especially, tapering along the tower and the choice of cross section are examined by considering the dynamic behaviour of the structure.

In the study of Young-Moon Kim and Ki-Pyo You [8], tapering and cross-sectional effect on dynamic behaviour of the structure is investigated. Most modern buildings have tapering which leads them to be more slender and more flexible with low damping. These flexible tall structures are prone to the wind-induced dynamic loadings which are crucial for design of buildings. The aerodynamic modification in the shape of building by tapering along the height of the building leads to a change in the flow pattern around the building that can reduce wind induced excitations of tall buildings. In the same study, in order to

observe the tapering effect for reducing the wind-induced effect on the buildings, a high-frequency balance test is conducted. Four types of buildings with different tapering ratios are taken into consideration. After the tests are conducted, it is concluded that the tapering leads the wind-induced excitation response of the building to decrease [8].

In Karam Y. Maalawi's study, it is showed that the cross section properties of the tower, as well as tapering ratio, and rotor/nacelle inertia ratios are significant in design parameters. It is concluded that as tapering increases, frequency decreases. The towers that have completely conical shapes may have the maximum frequencies; however, these types of formations are not serviceable for adequate space at the top of the tower in order support the rotor/nacelle combination [9].

One of the most important threats for wind turbines is fatigue failure. Fatigue is a type of damage that is sudden and causes by cyclic loading on an element or the whole system. This type of failure can occur even under ultimate strength of the elements. Fatigue should be considered in long-term period designs.

In Paul S. Veers and Steven R. Winterstein's study [10], fatigue effect on the wind turbine reliability is examined. Cycling loading can cause damage to structural elements. With the rainflow-range load method, the fatigue loading amplitudes can be computed and it is possible to characterize the fatigue loading. In the rainflow method, the uncertainty in the cyclic loading can be characterized by small sets of descriptive statistics. Then, the uncertainty can be transferred to the fatigue life estimation [10].

Characterizing fatigue loading is very difficult. To conduct fatigue analysis, there is a need for a procedure to describe loads. There are several procedures for describing the cyclic loading in fatigue; one of them is the rainflow counting method. In this method, firstly, the loading time series are acquired from the computer simulation. Then, the time series are rainflow counted to identify the loadings. The rainflow counting method counts the stress in an irregular time series. Lastly, the cycles are grouped into bins. After the rainflow counting process, data are collected and used in the statistical models. Then, the uncertainties in the statistical results are reflected in the fatigue life time estimations. These

uncertainties can be fed into probabilistic analysis to determine the safety factor required to acquire the desired level of reliability [10].

In S.S Cho, H. Chang and K. W. Lee's study, the dependence of high tension bolts of fatigue limit is examined. High tension bolts are prone to fatigue damage in critical joints. Therefore, they should be taken into consideration at the design level. The choice of the dimension, size and strength of the bolts are important for the structural safety and serviceability. Additionally, the fatigue life of the bolt depends on different factors such as external loads, joint stiffness and structural configuration of the whole system. The finite element analysis can give more accurate and realistic results [11].

In J. D. Holmes' study [12], fatigue damage for structures in along-wind direction is considered. By making some assumptions, closed-form approaches for upper and lower limits for fatigue life are derived. The fluctuating behaviour of the wind causes a stochastic loading on the structure that can create resonance on the system or the sub-systems. When the along-wind excitation is the principle factor, the wide-band contribution is dominant for most structures, The fatigue failure does not occur frequently; however, stochastic wind loading leads the designers to consider the fatigue in steel or aluminium structures that are exposed to turbulent wind loads [12].

1.2. Objective

In this study, a 5 MW onshore wind turbine was analyzed against fatigue failure at the bolted joints. Onshore wind turbines are prone to dynamic forces along their operational life. In this period, due to resonance, failure at various parts such as blades and connections can occur. Therefore, frequency of the excitation sources should be separate from structural frequency. These excitation sources are referred to as side-to-side which is due to unbalanced mass effect and fore-aft which is due to tower shadowing. In the unbalanced mass effect, one of the blades can have slightly different mass due to fabrication reasons; therefore, it leads to centrifugal excitation force. In the tower shadowing effect, as the blades rotate, each blade passes in front of the tower preventing wind from flowing across the tower at each turn.

In reality, actual structural frequency may be different than the analytical one due to uncertainties especially related with soil. This situation may result in resonance and the fatigue life of the structural parts changes significantly. Along this line, soil uncertainty is investigated in terms of soil stiffness that is represented by subgrade reaction of modulus.

Therefore, the main objective of this study is to show the importance of resonance effects in terms of fatigue life.

1.3. Scope

In Chapter 2, brief information about wind energy, historical development of wind turbines, total wind energy capacity and wind energy production of the World and Turkey is given.

In Chapter 3, 5 MW onshore wind turbine's properties are represented (i.e. the tower geometry, rotor diameter and weight, cut-in and cut-out speeds, hub properties). Detailed Finite Element Model (FEM) of the structure including soil springs is created and the corresponding modal values are obtained. Soil medium surrounding the foundation is represented by lateral and vertical soil springs attached to the mat foundation. This model is created and analyzed in the SAP 2000 software program.

In Chapter 4, a 5 MW onshore wind turbine model is created in the FAST (Fatigue, Aerodynamics, Structures and Turbulence) program which is a tool that can perform dynamic analyses for wind turbines. Effect of resonance is investigated in terms of base shear and over turning moment obtained from FAST analysis.

In Chapter 5, fatigue analysis is carried out by means of analytical solutions in which MS Excel platform is used. Afterwards, the resonance effect on fatigue life is discussed in comparative terms.

2. WIND ENERGY

Wind is the movement of the air crossing over the surface of the Earth, from areas of high pressure to low pressure. Uneven heating of the surface of the Earth by the Sun and the rotation of the Earth that drags the atmosphere are the main causes that create these pressure differentials [13].

Wind energy is the most convenient form energy in the renewable energy sources. and wind energy is transformed into a useful form of power by windmills and wind turbines.

The history of wind power indicates an evolution from the use of simple, light devices driven by aerodynamic forces; to heavy, material-intensive drag devices; to the increased material-efficient aerodynamic lift devices in the modern era [14].

2.1. History of Wind Energy

Historically the earliest known wind turbine design is “panemone windmill” which is a type of vertical axis turbine. It is made with vertical sails made of bundles of reeds that are attached to the central shaft by horizontal struts. It has a rotating axis position, while the blades move parallel to the wind. Therefore, it uses the drag force of the wind. In the Persian panemone design, the rotor can harvest only half of the striking wind. On the other hand, the shaft of a horizontal axis wind turbine points into the wind while the blades move at right-angles to the wind thrust. Therefore, the horizontal axis models use the lift forces of the wind [14, 15, 16].

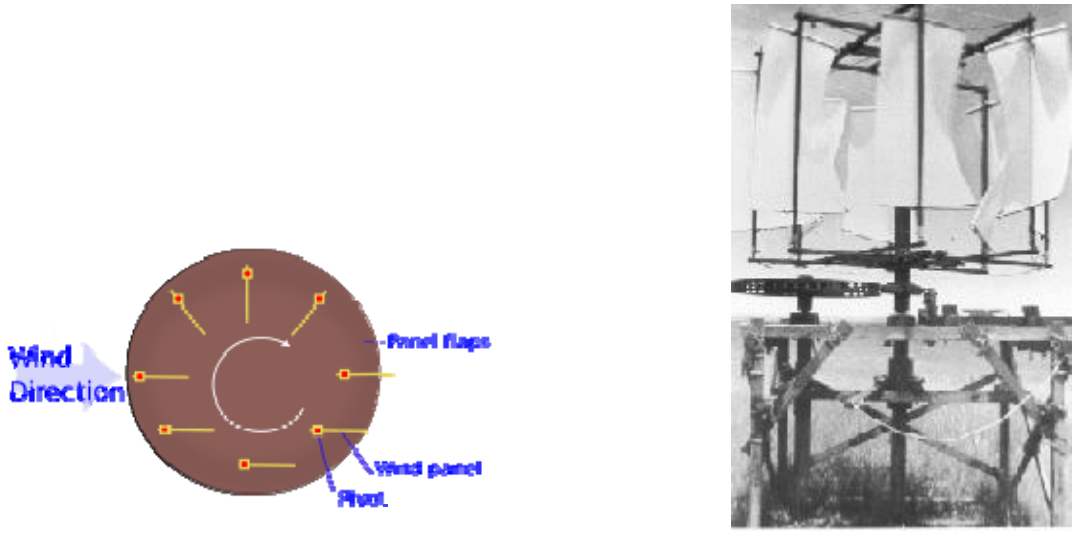

Figure 2.1. Early examples of wind turbines: a) working principle for Panemone design [16], b) A 19th century American made Panemone design [14].

The first windmills in the European region were made with a horizontal-axis configuration. The European water wheels also had a horizontal axis-configuration. The reason might be the higher-structural efficiency of drag type horizontal machines, due to the loss of half of the drag force in harvesting the wind [14].

In the early 1390s, Dutch people set out to refine the tower mill design. The Dutch affixed the standard post mill to the top of a multi-story tower. Both the post mill and the tower mill design had to be oriented into the wind manually, by pushing the lever at the back of the mill. Optimizing the wind mill energy, power output and protecting the mill from damage of the strong storms were the main problems [14].

Figure 2.2. A Dutch mill [14].

A primary improvement for the European mills was the aerodynamic lift generating design that can be seen in Figure 2.2. This feature enables improved rotor efficiency that allows for an increase in rotor speed much more than Persian mills and which also allows for superior grinding and pumping actions. [14]

The process of perfecting the windmill sails took over 500 years from the aforementioned time. By the time the process was completed, some essential features related to the blades had been considered by modern designers such as;

- Camber along the leading edge
- Placement of the blade spar at the quarter chord position
- Center of gravity at the same quarter chord location
- Non-linear twist of the blade from root to tip [14].

Some models also featured aerodynamic brakes, spoilers and flaps. The windmill that is shown in Figure 2.2 features leading edge airfoil sections [14].

Between 1850 and 1970, over six million mechanical output windmills were constructed in the U.S. alone. The primary use was pumping water for irrigation and stocking the water for farms and homes. In the late 19th century, the successful multi-blade windmill design was used to generate electricity. In the 1890s, a Danish scientist, Poul la Cour, constructed wind turbines to generate electricity, which was then used to produce hydrogen for experiments and light [14, 15].

The first small electrical-output wind turbines simply used modified propellers to drive direct current generators. By the mid 1920s, 1 to 3 kW wind generators were developed. The development of bulk power, utility-scale wind-energy systems was first done in Russia in 1931 with the 100 kW Balaclava wind generator that operated about two years [14].

In 1931, the Darrieus wind turbine was invented with its vertical axis providing a different mix of design tradeoffs from the horizontal axis wind turbines. One of the most important Darrieus designs was a modern-type rotor comprising slender, curved, airfoil section blades attached at the top. The Darrieus design enabled the velocity of the vertical axis wind turbine blades to increase significantly above the wind velocity so that lift forces could be used to improve the performance of the turbines since their designs are based on drag [14, 15, 17].

The world's first mega-watt sized wind turbine was constructed in 1941 and was connected to the electrical distribution system in Vermont, US as shown in Figure 2.3. This 1.25 MW turbine operated for 1100 hours before a blade failed at a weak point [15].

Figure 2.3. First-megawatt sized turbine [15].

2.2. Renewable Energy and Wind Energy

Renewable energy comes from natural resources such as sunlight, rain, tides, geothermal heat and wind which can be renewed [18]. The production of renewable energy accounts for a significant share of the global energy sector.

Renewable energy has been replacing the other types of energies such as fossil and nuclear fuels in many distinct markets such as power generation, heating and cooling, etc. Renewables are becoming increasingly essential especially in the transportation and heating sectors [19].

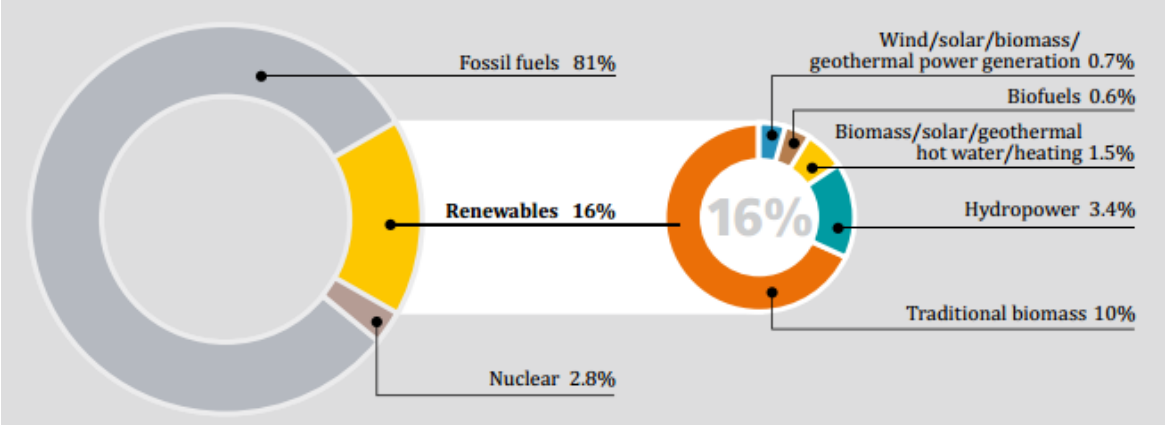

Figure 2.4. Renewable Energy Share of Global Final Energy Consumption, 2009 [19].

Figure 2.4 shows that renewable energy consumption takes a 16% share of global energy consumption. Existing renewable power capacity in 2010 reached approximately 1320 gigawatts, up almost 8% from 2009. In this 16% slice, traditional biomass takes the largest place with 10%. Wind/solar/biomass/geothermal power generation energies take a 0.7% share [19].

Since the end of 2004, worldwide energy capacity has been growing with an annual rate of 10-60%. For wind power, growth accelerated in 2009 relative to the other four years. It is expected that by 2014, installed capacity of photovoltaics will exceed that of wind, but due to the lower capacity factor of solar power, the electric production will not exceed that of wind capacity [18, 19]. The investment and the capacities of different renewable energies are given in Table 2.1 and 2.2.

Table 2.1. Investments and capacities in renewable energies [19].

SELECTED INDICATORS	units	2008	2009	2010
Global new investment in renewable energy (annual)	Billion USD	130	160	211
Renewables power capacity (existing, not including hydro)	GW	200	250	312
Renewables power capacity (existing, including hydro)	GW	1150	1230	1320
Hydropower capacity (existing)	GW	950	980	1010
Wind power capacity (existing)	GW	121	159	198
Solar PV capacity (existing)	GW	16	23	40
Solar PV cell production (annual)	GW	6.9	11	24
Solar hot water capacity (existing)	GW_{th}	130	160	185
Ethanol production (annual)	Billion liters	67	76	86
Biodiesel production (annual)	Billion liters	12	17	19
Countries with policy targets	#	79	89	98
States/provinces/countries with feed-in policies	#	71	82	87
States/provinces/countries with RPS/quota policies	#	60	61	63
States/provinces/countries with biofuels mandates	#	55	57	60

The global new investment in renewable energy reached 260 billion USD in 2011 [20].

Table 2.2. Existing capacities as of end-2010 in top five countries [19].

	Renewables power capacity (not including hydro)	Renewables power capacity (including hydro)	Wind power	Biomass power	Geothermal power	Solar PV	Solar hot water/heat
1	United States	China	China	United States	United States	Germany	China
2	China	United States	United States	Brazil	Philippines	Spain	Turkey
3	Germany	Canada	Germany	Germany	Indonesia	Japan	Germany
4	Spain	Brazil	Spain	China	Mexico	Italy	Japan
5	India	Germany/ India	India	Sweden	Italy	United States	Greece

The energy need of the world has increased especially in this century. Thus, this need has to be met by certain resources. During the middle and even the end of the last century, the main concern was for the energy supply to be as cheap as possible. However, the world has begun to realize that the demand must be met in an environmentally friendly and cheap way at the same time. These characteristics point out wind power which has almost no

pollution or global warming effects, and no fuel cost. That's why wind energy sources have gained an outstanding significance all around the world.

Figure 2.5 shows the change in global wind power cumulative capacity in GW from 1996 to end of 2010.

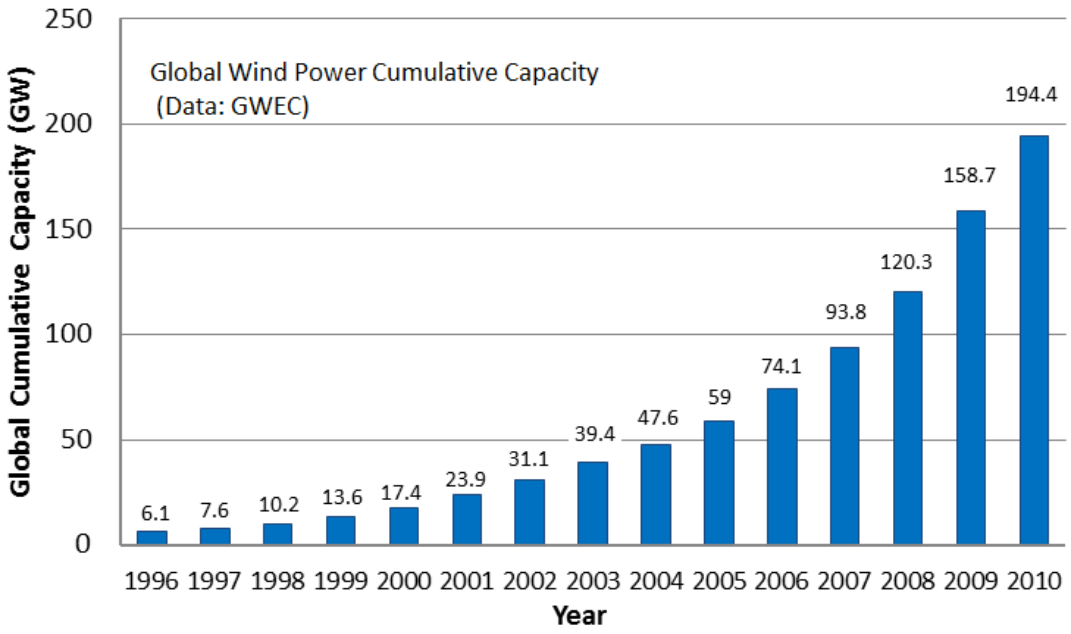

Figure 2.5. Global Wind Power Cumulative Capacity [20].

Figure 2.6 shows top 10 country in cumulative wind energy capacity and new installed wind energy capacities in 2010.

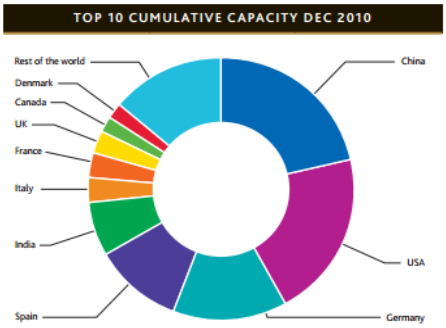

Country	MW	%
China	42,287	21.8
USA	40,180	20.7
Germany	27,214	14.0
Spain	20,676	10.6
India	13,065	6.7
Italy	5,797	3.0
France	5,660	2.9
UK	5,204	2.7
Canada	4,009	2.1
Denmark	3,752	1.9
Rest of the world	26,546	13.7
Total TOP 10	**167,844**	**86.3**
World Total	**194,390**	**100**

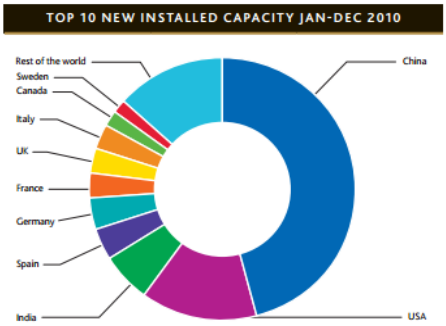

Country	MW	%
China	16,500	46.1
USA	5,115	14.3
India	2,139	6.0
Spain	1,516	4.2
Germany	1,493	4.2
France	1,086	3.0
UK	962	2.7
Italy	948	2.6
Canada	690	1.9
Sweden	603	1.7
Rest of the world	4,750	13.3
Total TOP 10	**31,052**	**86.3**
World Total	**35,802**	**100**

Figure 2.6. Top 10 Total Installed wind turbine capacity in 2010 [20].

According to the Republic of Turkey Energy Market Regulatory Authority (EMRA), the annual energy need of Turkey was illustrated in Table 2.3 [21].

Table 2.3. Annual energy need of Turkey according to EMRA [21].

Years	**Annual Energy Demand (GWh)**	**Increase wrt 2001**	**Increase wrt Previous Year**
2001	126871	-	-
2002	132553	4.48%	4.48%
2003	141151	11.26%	6.49%
2004	150018	18.24%	6.28%
2005	160794	26.74%	7.18%
2006	174637	37.65%	8.61%
2007	190000	49.76%	8.80%
2008	198085	56.13%	4.26%
2009	194079	52.97%	-2.02%
2010	210434	65.86%	8.43%

Energy need of Turkey in 2010 was more than one and a half of that of the annual demand 2001. Reasons for this increase in energy were the rapidly growing economy and population, and political stability, which stimulated investors to invest more [21].

Before 1997, wind power production was almost zero. However, Turkey has a significant wind power potential that is seen in Figure 2.7. After this date, energy produced from wind power plant has increased and this is shown in Table 2.4 [21].

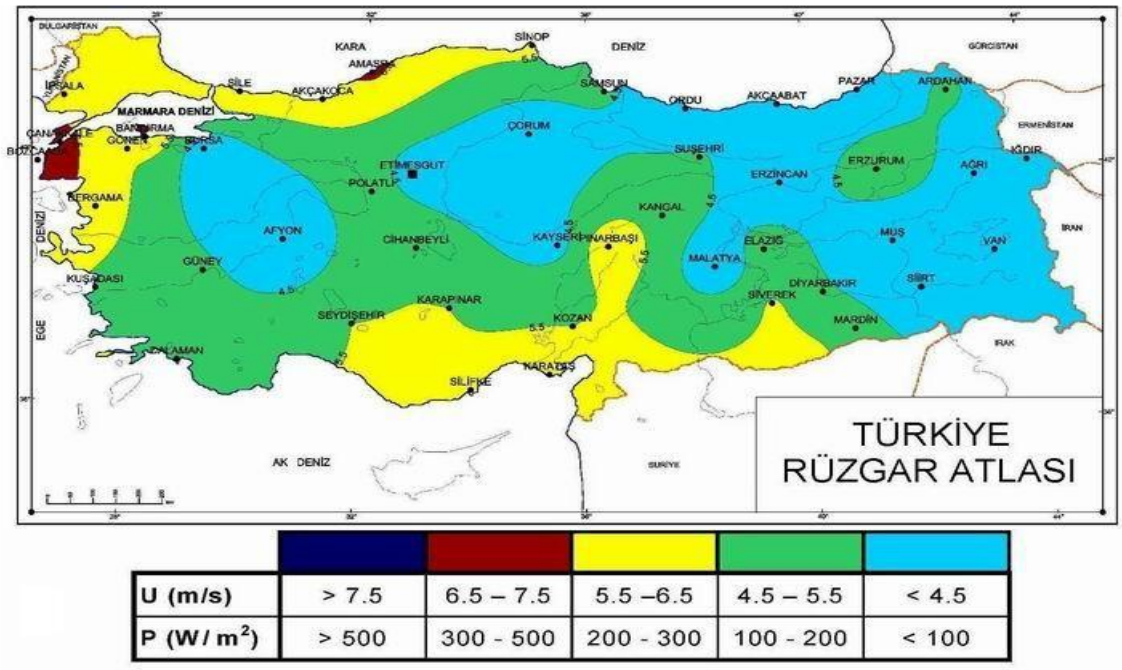

Figure 2.7. Wind Speed Map of Turkey for the height of 50 m [22].

Table 2.4. Wind Energy and Total Energy Comparison between 1997 and 2010 [21].

	Wind Energy (MW)	**Total Energy (MW)**	**Share in the year**
1997	0.0	21891.9	0.00%
1998	8.7	23354.0	0.04%
1999	8.7	26119.3	0.03%
2000	18.9	27264.1	0.07%
2001	18.9	28332.4	0.07%
2002	18.9	31845.8	0.06%
2003	18.9	53387.0	0.04%
2004	18.9	36824.0	0.05%

Table 2.4. Wind Energy and Total Energy Comparison between 1997 and 2010 (cont.) [21].

	Wind Energy (MW)	Total Energy (MW)	Share in the year
2005	20.1	38843.5	0.05%
2006	20.1	40564.8	0.05%
2007	92.0	40835.8	0.23%
2008	316.3	41817.2	0.76%
2009	791.6	44761.2	1.77%
2010	1320.2	49524.1	2.67%

Table 2.5 shows , the share of installed capacity of wind power in the total installed capacity as of 2010 [21]:

Table 2.5. The share of installed capacity of wind power [21].

	Installed Capacity	Share in Total
Thermal	32278.5	65.18%
Hydraulic	15831.2	31.97%
Geothermal	94.2	0.19%
Wind	1320.2	2.67%
Total	49524.1	

Compared with the total wind power generation of the world, Turkey has begun to increase its wind energy generation share as shown in Table 2.6 [21].

Table 2.6. Comparison of total wind energy generation of Turkey in the World [21].

	2005	2006	2007	2008	2009	2010	2011
Total Wind Energy Generation of the World	59091	74052	93835	120798	158700	194400	237669
Total Wind Energy Generation of Turkey	0.0201	0.0201	0.092	0.316	0.7916	1.3202	1.491
Share %	0.00003	0.00003	0.00010	0.00026	0.00050	0.00068	0.00063

Now, the EMRA has forecasted total produced energy and wind energy for each year and the results are shown in the Table 2.7 [21].

Table 2.7. Forecasts of EMRA about Wind Energy and Total Energy for 2015 [21].

		Wind Energy (MW)	**Total Energy (MW)**	**Share in the year**	**Increase wrt 2010**
Actual	**2010**	1320.2	49524.1	2.67%	-
Forecasted	**2011**	1491.0	53034.8	2.81%	12.94%
Forecasted	**2012**	1965.0	55321.8	3.55%	48.84%
Forecasted	**2013**	3328.0	62379.8	5.34%	152.08%
Forecasted	**2014**	3328.0	65206.8	5.10%	152.08%
Forecasted	**2015**	3328.0	66406.8	5.01%	152.08%

All in all, the wind power generation of Turkey will be expected to increase.

3. MODELLING

In this part, the system properties and the structural models of the onshore wind turbine system is described. The calculation of the modulus of subgrade reaction values and the creation of the foundation model are also given in this chapter.

3.1. General Description

A figure for an onshore wind turbine that is used in this thesis is shown in Figure 3.1.

Figure 3.1. Figure for a 5MW onshore wind turbine [23].

The mechanical section is the nacelle-rotor part which is assembled at the top of the tower. The electrical power is generated as the blades are rotated; afterwards it is transmitted by the national grid which is connected to the tower at the foundation level.

Figure 3.2. Rotor-nacelle assembly [24].

3.1.1. Tower properties

In this thesis, NREL's Baseline 5 MW wind turbine model, which is called Repower 5M, is used. The main properties are listed in Table 3.1 to Table 3.4.

Table 3.1. General properties of the 5 MW Wind Turbine

Rating	5 MW
Rotor Orientation, Configuration	Upwind, 3 Blades
Rotor, Hub Diameter	126 m, 3 m
Hub Height	90 m
Cut-in, Rated, Cut Out Wind Speed	3 m/s, 11.4 m/s, 25 m/s
Cut-in, Rated Rotor Speed	6.9 rpm, 12.1 rpm
Rated Tip Speed	80 m/s
Overhang, Shaft Tilt, Precone	5 m, 5^0, 2.5^0
Rotor Mass	110000 kg
Nacelle Mass	240000 kg
Tower Mass	277500 kg

Table 3.2 Blade properties

Length (w.r.t. Root Along Preconed Axis)	61.5 m
Overall (Integrated) Mass	17740 kg
CM Location (w.r.t. Root along Preconed Axis)	20.475 m
Structural-Damping Ratio (All Modes)	0.0048

Table 3.3 Nacelle and Hub Properties

Elevation of Yaw Bearing above Ground	87.6 m
Vertical Distance along Yaw Axis from Yaw Bearing to Shaft	1.96 m
Distance along Shaft from Hub Center to Yaw Axis	5.02 m
Distance along Shaft from Hub Center to Main Bearing	1.912 m
Hub Mass	56780 kg
Hub Inertia about Low-Speed Shaft	115926 $kg.m^2$
Nacelle Mass	240000 kg
Nacelle Inertia about Yaw Axis	2607890 $kg.m^2$
Nacelle CM Location Downwind of Yaw Axis	1.9 m
Nacelle CM Location above Yaw Bearing	1.75 m
Equivalent Nacelle-Yaw-Actuator Linear-Spring Constant	9028320 kN.m/rad
Equivalent Nacelle-Yaw-Actuator Linear-Damping Constant	19.60 kN.m/(rad/s)

Table 3.4 Tower geometrical and physical properties

Tower-Top Height Above Ground Level	87.6 m
Tower-Base Height Above Ground Level	10 m
Tower Base Diameter	6 m
Tower Base thickness	0.027 m
Tower Top Diameter	3.87 m
Tower Top thickness	0.019 m
Young's Modulus of steel	210 Gpa
Shear Modulus of steel	80.8 Gpa
Steel density (effective)	8500 kg/m^3

3.1.2. Support structure properties

The support structure is a mat foundation of C40 concrete to which lateral and vertical soil springs are attached. The specific weight of the concrete is 2.4 t/m^3. Young's modulus of elasticity is 34000 MPa. The support structure properties are given in Table 3.5 and a representative one is shown in Figure 3.3

Table 3.5. Foundation properties

Type of the foundation	Concrete / Mat Foundation
Length / Width / Height of the foundation	15 m / 15 m / 3 m
Compressive strength	40 MPa
Young's modulus of concrete	34000 MPa
Poisson's ratio	0.3
Specific weight of concrete	2.4 ton/m^3

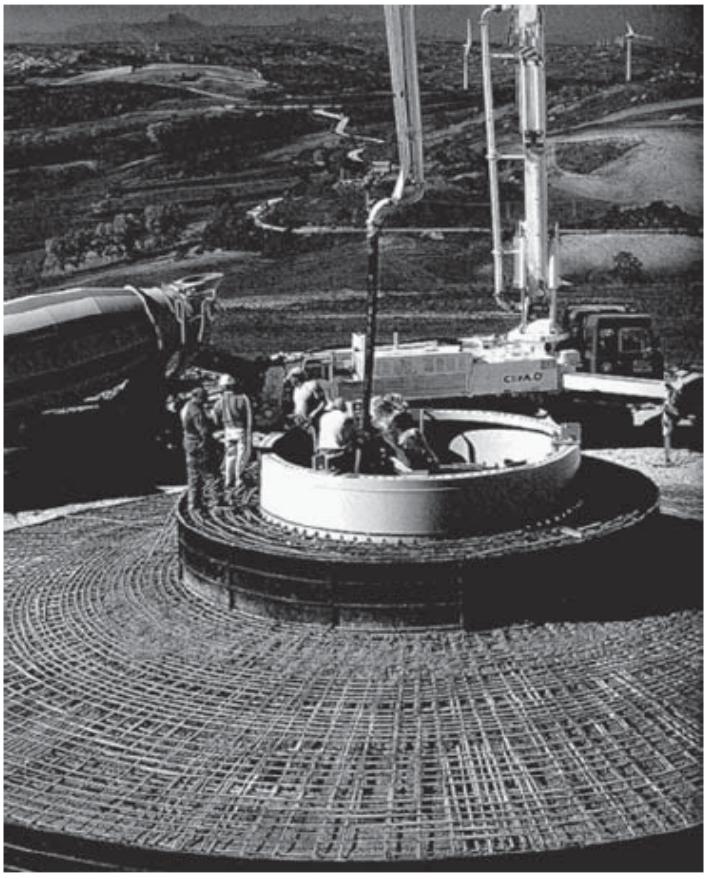

Figure 3.3. Example of a raft foundation of a wind turbine [17]

3.1.3. FAST, TurbSim and SAP 2000 Softwares

In the thesis, FAST and SAP 2000 programs are used to create wind turbine models and conduct static and dynamic analysis.

FAST (Fatigue, Aerodynamics, Structures and Turbulence) is an aerodynamic simulation program. Dynamic analysis of the 5 MW onshore wind turbine is conducted by FAST software. FAST has some auxiliary modules to carry out the dynamic analysis steps. The most important module is AeroDyn which is the aerodynamic module.

TurbSim code is a stochastic, full-field, turbulent-wind simulator. TurbSim is used for generation of the stochastic wind data. These data are integrated in the FAST program for dynamic analysis.

SAP 2000 is a structural analysis program. It is used for modelling of wind turbine tower and foundation. After the modal analysis of the system in the SAP 2000 program, mode shape results are integrated into FAST program. In Figure.. diagram for the methodolgy of the static and dynamic analysis of the wind turbine can be seen.

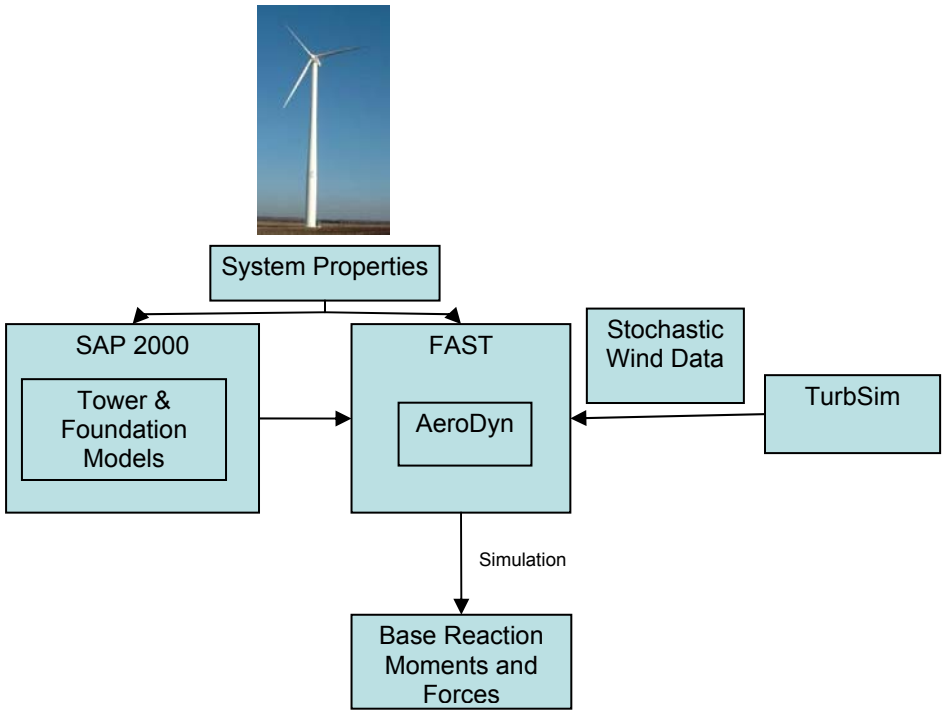

Figure 3.4. Static and Dynamic Analysis Diagram [43].

3.2 Wind Load

Wind load is the most critical loading for the wind turbine design. Due to stochastic nature of the wind, environmental data are collected at the given site. In another way, these data can be defined with some distribution functions. The TurbSim Code is used in this thesis for wind speed generation [25].

3.2.1. TurbSim Code

The TurbSim Code is a stochastic, full-field, turbulent-wind simulator. It numerically simulates time series of three-component wind-speed vectors at points in a two dimensional vertical rectangular grid that is fixed in space using a statistical model [25].

In the TurbSim simulation method, spectra of velocity and spatial coherence models are defined in the frequency domain and an inverse Fourier transformation produces time series compatible with FAST code [25].

In this thesis, the IEC Kaimal Spectral model which uses scaling parameters from IEC 61400-1, 3rd edition was used [25].

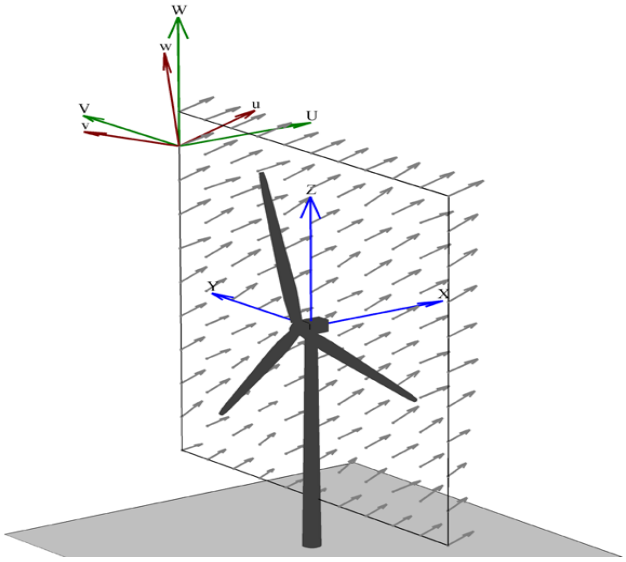

Figure 3.5. Diagram of a TurbSim wind field [25].

The velocity spectra, and also standard deviations of the IEC Kaimal Model are supposed to be invariant across the grid. However, in practice, a small amount of variation in the *u*-component standard deviation occurs because of the spatial coherence model. Furthermore, the Class I turbulent Extreme Turbulence Model was used for the turbulence type of the turbine using a 10 minute average wind speed and with a reccurrence period of 1 year [25].

TurbSim uses a parameter which is called ScaleIEC to scale the time-domain velocity output of the IEC Kaimal spectral model. Through this scaling, turbulence intensity and spectral models get more reasonable values. Also, TurbSim uses different random seeds to produce a Gaussian distribution of turbulence intensity in the longitudinal wind component, resulting from spatial coherence. A TurbSim wind field has a rectangular shape and it has a location (tower height) and dimensions [25].

Figure 3.6. Grid points for the wind velocity [26].

3.2.2. Formation of Wind Speed

In this thesis, wind is considered as a long term formation. Wind speed has variation and it can be described by different distribution models. Due to the turbulence velocity fluctuations about the mean speed and dynamic structural response,. TurbSim uses Gaussian distribution to generate the wind data [25].

In the probability theory, the Gaussian distribution is known as a continuous probability distribution which has a bell shaped probability density function:

$$f(x;\mu;\sigma^2)=\frac{1}{\sigma\sqrt{2\pi}}e^{-\frac{1}{2}\left(\frac{x-\mu}{\sigma}\right)^2}$$

Where μ is mean or expectation (location of the peak) and σ is standard deviation.

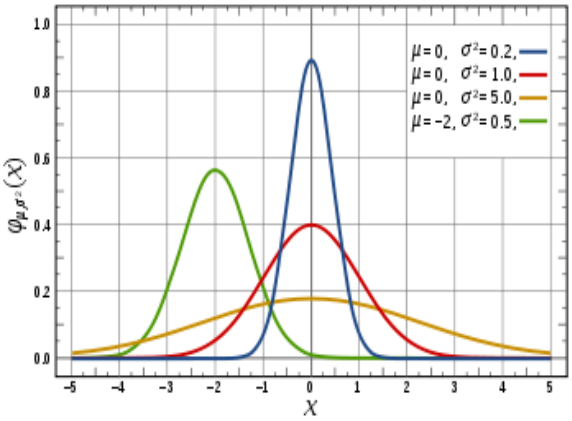

Figure 3.7. Probability density function [27].

3.2.3 Wind on Blades

According to the wind speed, the blades can open or close themselves against the wind. When the wind speed is higher than the value of 3 m/s, the blades open up to start to operate. When the wind speed reaches the value of 11.4 m/s, the blades operate in a constant rotational speed of rotor. In the probability of occurrence, there may be an extreme wind speed and also storm effects on the turbine. In the case of a wind speed above 25 m/s, to prevent damage of any kind to the unit or the whole system, the turbine takes a parked position. It means that the blades rotate along the cord length to the 90^0 position. 3 m/s wind speed is called cut-in, 25 m/s wind speed is called cut-out wind speed in the 5MW reference wind turbine as shown in Figure 3.7.

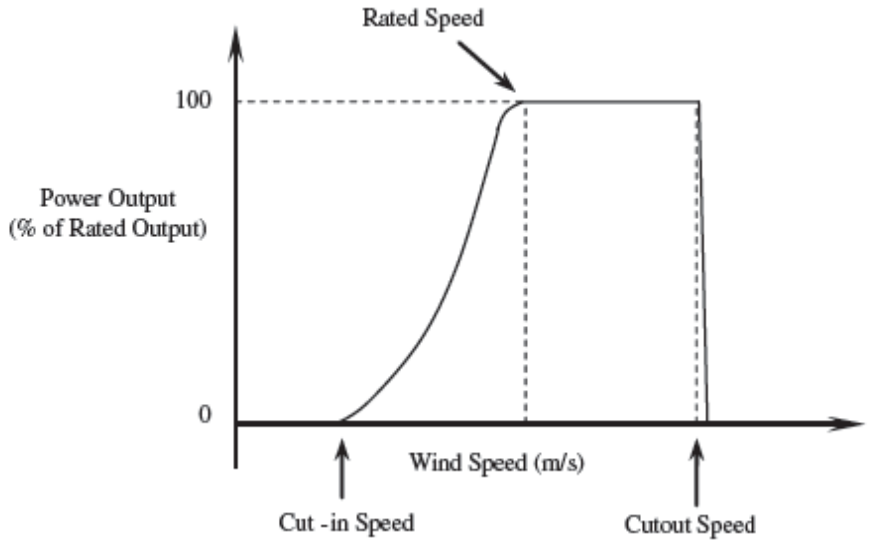

Figure 3.8. Typical wind turbine power curve [17].

When the wind flow coincides with the blades, two main forces namely lift and drag forces occur, and these forces can be described by the Blade Element Momentum Theory.

3.2.4. Blade Element Momentum Theory and Element Forces

The Blade Element Momentum Theory equates two methods of examining how a wind turbine operates. The first method uses a momentum balance on a rotating annular stream tube passing through a turbine. The second method is examining the forces produced by the aerofoil lift and drag coefficients at various sections along the blade section [28].

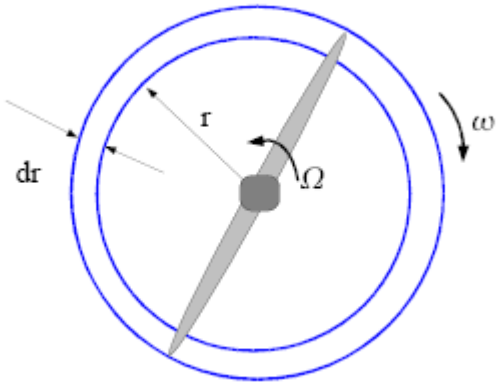

Figure 3.9. Rotating annular Stream tube [28].

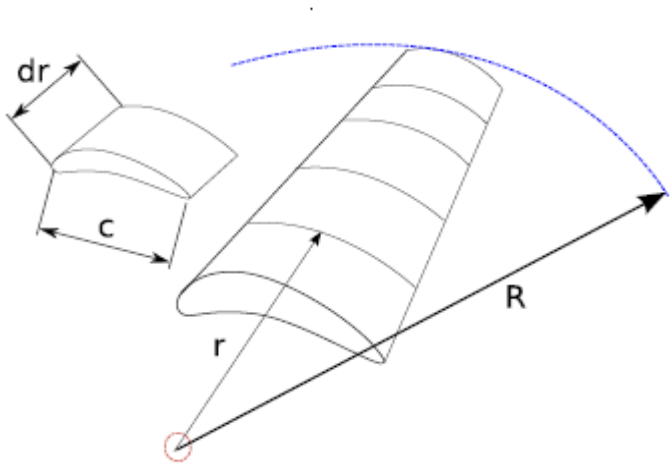

Figure 3.10. Blade Element Model [28].

The blade element momentum theory has two fundamental assumptions:

- There is not any aerodynamic interaction between different blade elements.
- The forces on the blade elements are determined only by the lift and drag coefficients [28].

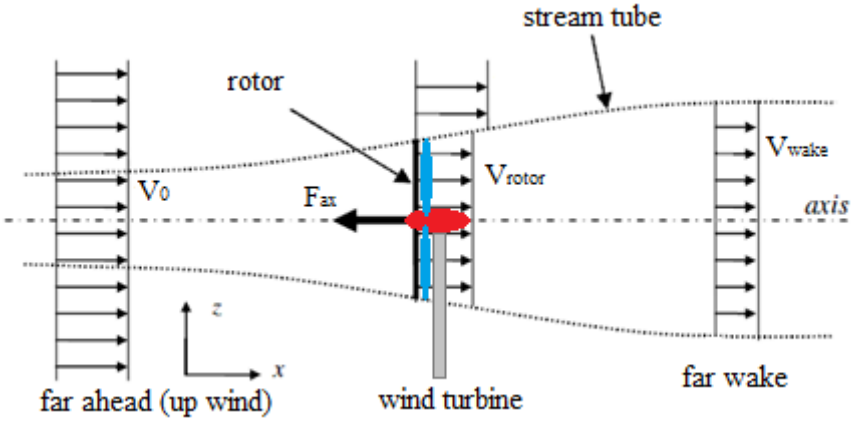

Figure 3.11. Rotor model with stream tube [29].

By using the Bernoulli equation, the resulting load on the actuator disk (rotor) can be calculated as [30]:

$$F_{ax} = \frac{1}{2} A_{rotor} \rho_{air} V_0^{\,2} * 4a(1-a)$$

Where α is induction factor, V_0 is wind velocity in m/s, V_{rotor} is wind velocity at the rotor, in m/s, ρ_{air} is air density in kg/m^3, A_{rotor} is area of the rotor disk in m^2.

The wind force on a blade element can be computed as [30]:

$$F_{wind} = \frac{1}{2} C_s \rho_{air} A V_{rotor}^2$$

Where F_{wind} is wind load in N, C_s is aerodynamic coefficient (shape) that is taken as 0.7, A is exposed area, in m.

To find the aerodynamic loads on the blades, the relative wind should be introduced which is [29]:

$$V_{rel} = \sqrt{V_{disk}^2 + V_{rot}^2}$$

$$V_{disk} = V_0(1-a) \text{ and } V_{rot} = \Omega * r$$

Where V_{rel} is relative wind speed at a blade section in m/s, V_{disk} is wind velocity at airfoil in m/s, V_{rot} is linear rotation speed at a blade section in m/s, Ω is angular rotational speed in rad/s, r is distance of a blade element to axis of rotation in m.

The airfoil profile is shown in the figure below.

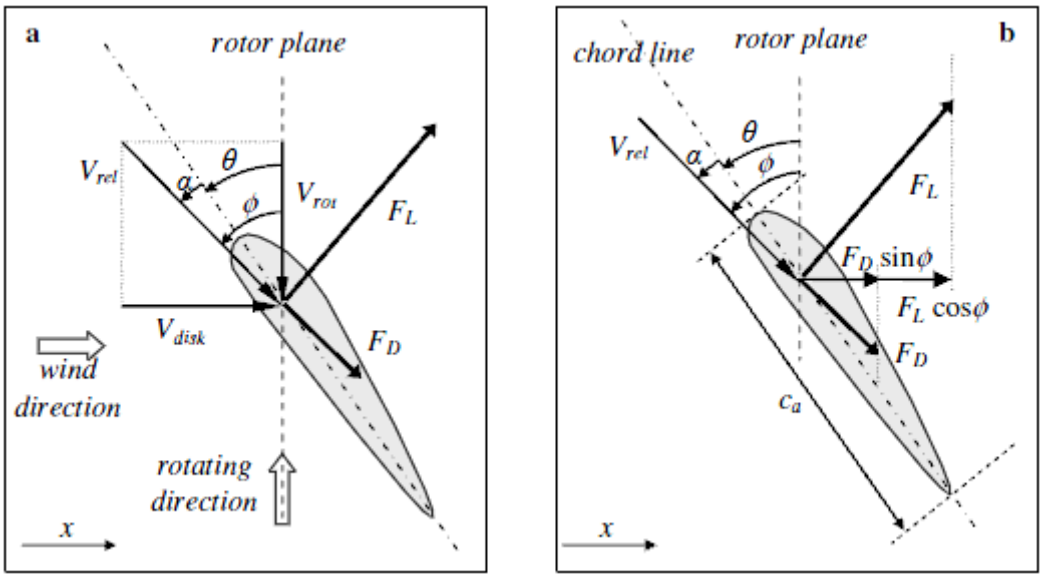

Figure 3. 12. a) lift and drag forces on the blade element b) resulting loads in x direction [29].

$$F_L = \frac{1}{2} C_L(\alpha) \rho_{air} V_{rel}^2 c_\alpha \Delta r \qquad F_D = \frac{1}{2} C_D(\alpha) \rho_{air} V_{rel}^2 c_\alpha \Delta r \quad [29]$$

Where F_L is aerodynamic lift force in N, F_D= aerodynamic drag force in N, $C_L(\alpha)$ is aerodynamic lift coefficient, $C_D(\alpha)$ is aerodynamic drag coefficient, c_α is airfoil chord length in m, Δ_r is radial length of blade element in m, α is angle of attack in deg, Θ is pitch angle in deg, Ø is angle of inflow in deg.

Load in x direction in one blade element is:

$$F_x = F_L \cos\phi + F_D \sin\phi$$

Total axial load is [30]:

$$F_{ax} = N_b \sum_{r=root}^{r=tip} F_{x,r}$$

3.3. Tower modelling

In the FAST program, the structure is defined as a cantilever beam that the tower is fictionally extended at a certain level to have the same natural frequency as the model that includes a mat foundation.

In the SAP 2000 model, after the modal analysis, we aquire mode shapes for the side to side and fore-aft cases. In the Figure 3.12, we can observe the first and second mode shapes for the wind turbine model with effective fixity. In the FAST program, dynamic response is represented by the first and second modes for each cases.

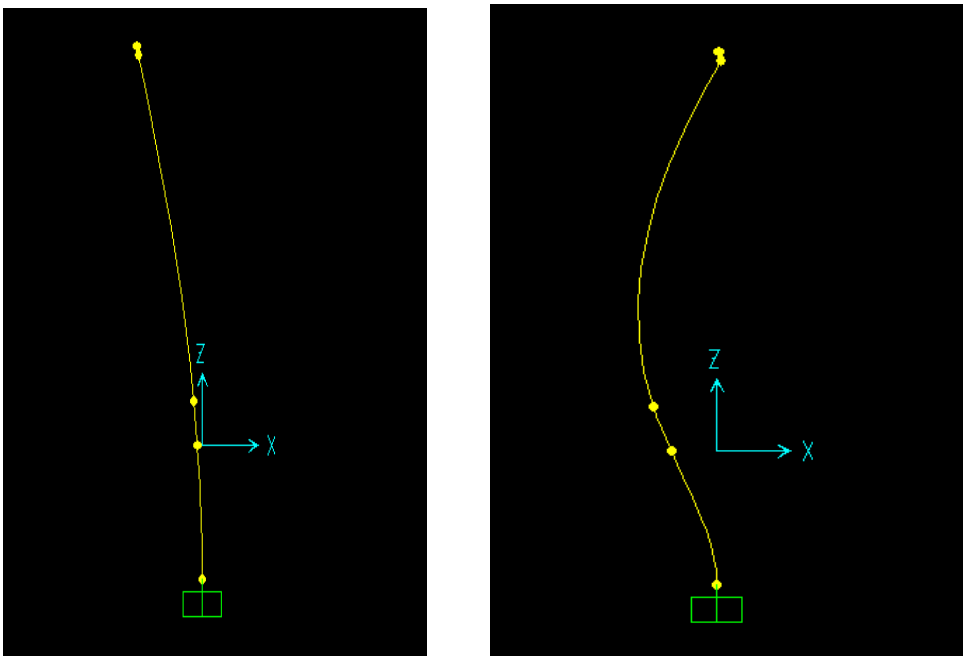

Figure 3.13. a) 1st mode of the tower, b) 2nd mode of the tower

3.4. Foundation modelling

In the FAST program, the support platform properties can be entered as the physical and geometrical values. However, the onshore foundation case is included only in the fixed bottom concept. Therefore, first we should model the onshore foundation and tower, then transform this model to the fixed-bottom type of tower that have the same natural frequencies, called effective fixity. Figure 3.13 shows an onshore wind turbine model.

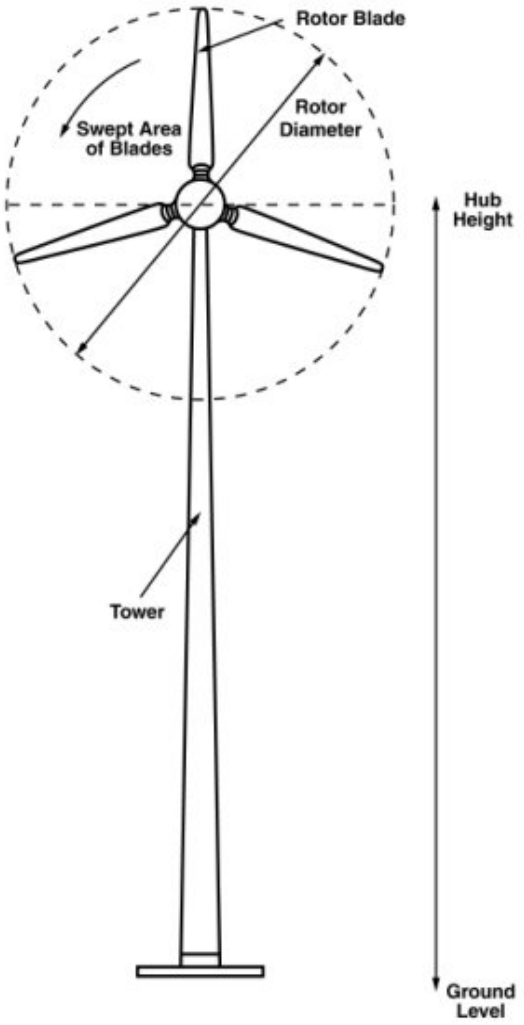

Figure 3.14. Wind turbine model [31].

3.4.1. SAP 2000 Modelling

Figure 3.14 shows onshore mat foundation and effective fixity models which are created in SAP 2000 program.

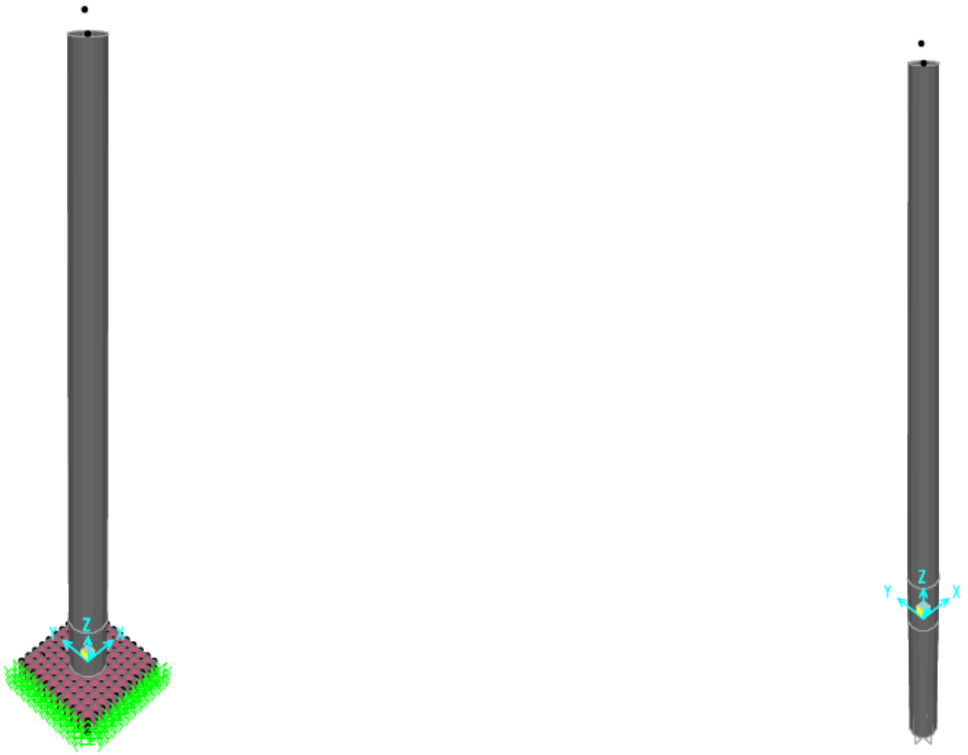

Figure 3.15. Onshore mat foundation and effective fixity models.

In the mat foundation modelling, elastic springs are introduced laterally and vertically to represent the soil effect. These are called p-y (lateral) and t-z (vertical) springs.

In the effective fixity model, the tower is extended beyond the soil with a certain fictitious length to get the same natural frequency as the model that has mat foundation. Thus, we introduce a fixed-bottom onshore model into the FAST input file with its geometrical properties.

3.4.2. Modulus of Subgrade Reaction Check

In this part, modulus of subgrade reaction of soil surrounding foundation is analyzed. For the purpose of this study, a dense sand soil example is chosen. With the aim of getting an approximate modulus of subgrade reaction value, a common formula is used which is given below:

$$k = \frac{p}{y}.$$

Where k is modulus of subgrade reaction in kN/m^3, p is net pressure per unit area of the foundation in kN/m^2, y is settlement produced by applied load in m.

In this equation, the value of p can be found by the dead load calculation of the upper part of the structure which includes the tower and the nacelle-rotor systems. However, the settlement should be found with some calculations using certain theorems as the Boussinessq Theorem.

Settlement calculation is taken into consideration as long term consolidation, to get a long term representative subgrade reaction value. In the below equation the long term settlement can be calculated as:

$$S_{oed} = m_v * \Delta H * \Delta q$$

Where S_{oed} is settlement value in m, m_v is coefficient of volume compressibility in m^2/kN, ΔH is thickness of the compressible layer in m, Δq is average stress increment in compressible layer in kN/m^2.

In this equation; m_v value is chosen for dense sand as $1.5x10^{-5}$ m^2/kN and ΔH is chosen as 20 m. Δq can be found by the Boussinessq Theorem which is given as the approximate 2:1 method.

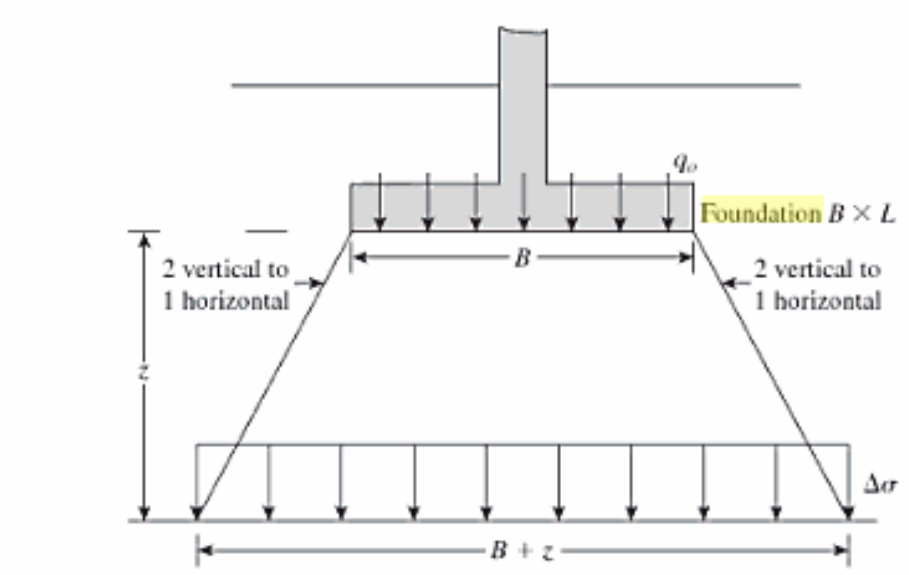

Figure 3.16. 2:1 method of finding stress increase under a foundation [33].

$$\Delta\sigma = \frac{q_0 BL}{(B+z)(L+z)}$$

Where q_0 is net pressure on the foundation area in kN/m^2, L is length of the foundation in m, B is width of the foundation in m, Z is depth of the soil layer in m, $\Delta\sigma$ is average stress increment at the layer in kN/m^2.

The dead load of the structure above the foundation is given as:

Tower top mass is 350 tons = 3434 kN.

The tower structure mass is 277.5 tons = 2723 kN.

Foundation mass is 1620 tons = 15892 kN

Total weight is 3434+2723+15892 = 22049 kN.

Net pressure on the foundation area is:

$$p = \frac{Q}{A} = \frac{22049}{(15 \times 15)} = 98.00 \text{ kN/m}^2$$

$$\Delta\sigma = \left(\frac{98.00 \times 15 \times 15}{(15+20) \times (15+20)} \right) = 18.00 \text{ kN/m}^2$$

According to the settlement formulation:

$$S_{oed} = m_v * \Delta H * \Delta q$$

$$S_{oed} = \left(1.5 \times 10^{-5}\right) \times 20 \times 18.00 = 5.4\text{x}10^{-3} \text{ m.}$$

Approximately 5.4 mm settlement occurs in a long term period of consolidation.

According to the formulation in Terzaghi's study [32];

$$k = \frac{p}{y}$$

$$\text{k} = \frac{98{,}00}{5{,}4 \times 10^{-3}} = 18148 \text{ kN/m}^3$$

In Terzaghi's study of shallow foundations, in a square footing in granular soils:

$$k_B = k_{30} \cdot \left(\frac{B + 0.3}{2B} \right)^2$$

Where k_B is appropriate subgrade reaction value in kN/m^3, k_{30} is the subgrade reaction value obtained from the Boussinessq Theory in kN/m^3, B is length of the footing in m.

$$k_B = 18148 \times \left(\frac{15 + 0.3}{2 \times 15} \right)^2 = 4720 \text{ kN/m}^3$$

In the foundation model of this thesis, the area is 15 x 15 = 225 m^2. The one dimensional spring coefficient is:

4720 kN/m^3 x 225 m^2 = 1062000 kN/m.

Lateral soil spring is taken as two thirds of vertical spring.

Figure 3.16 shows representation of the lateral and vertical soil springs. In this model, mesh dimensions are 1.5 m x 1.5 m. Total spring coefficient is divided by 2.25 to acquire the corresponding value at each mesh and afterwards, that value is distributed to each corners of square meshes.

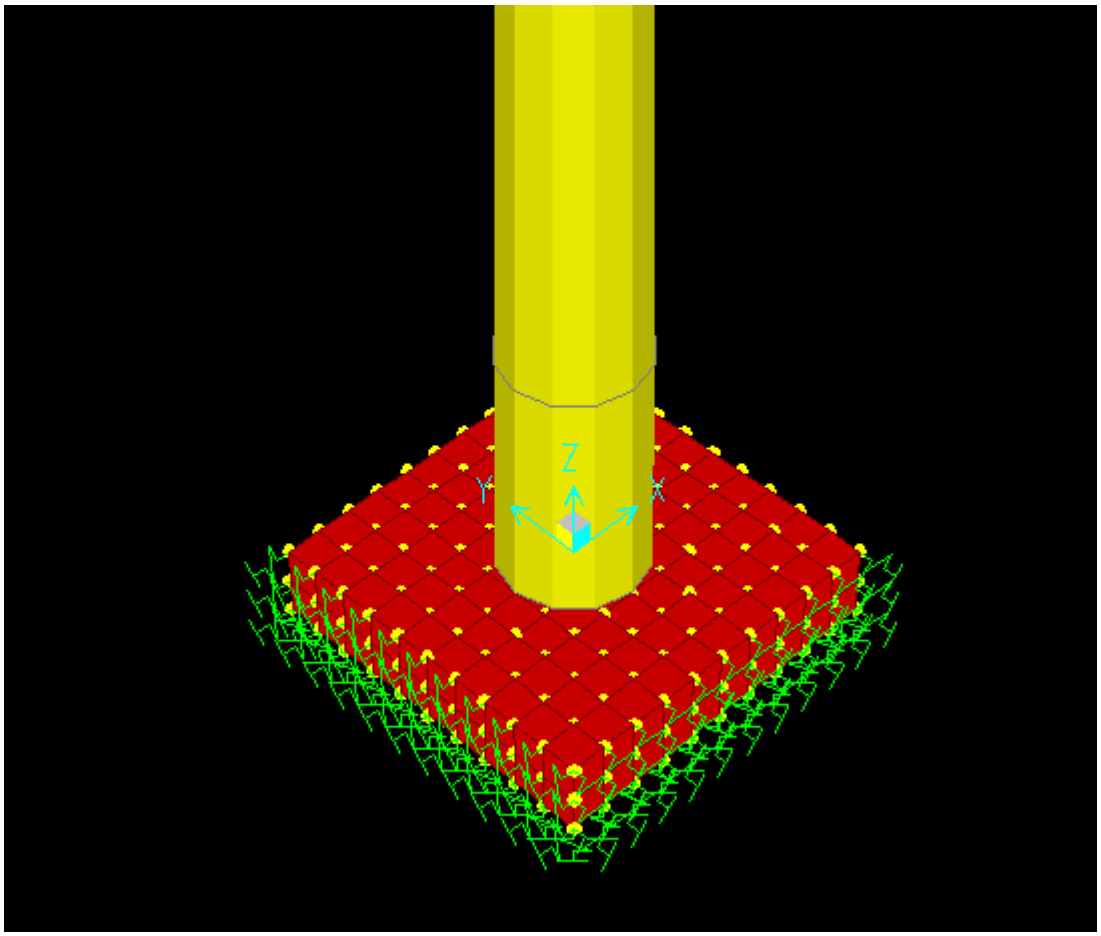

Figure 3.17. Foundation model with springs in SAP 2000.

3.4.3. Parametric Study for Modulus of Subgrade Reaction

In this part, a parametric study has been carried out and plotted as shown in Figure 3.17. As can be seen from this figure, by decreasing soil stiffness values to the half of their original value i.e. from 15000 kN/m^3 to 7500 kN/m^3, the overall structural period elongates from 4.15 sec to 4.69 sec. In the 4.69 sec model the foundation subgrade reaction in a vertical direction totals 744000 kN/m, which is closer to medium sand values.

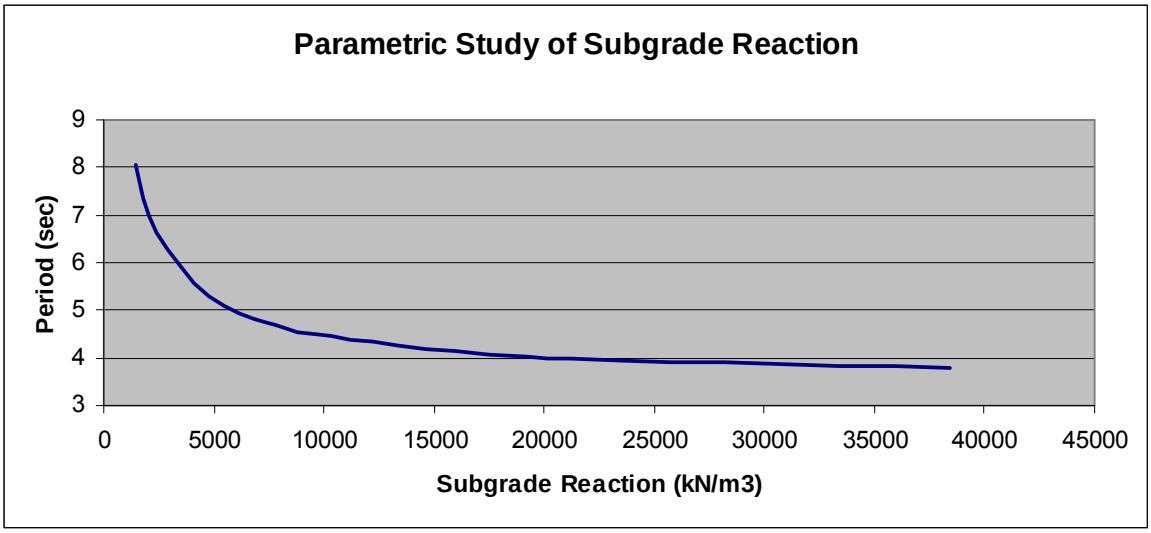

Figure 3.18. Graph of the parametric study for Modulus of Subgrade Reaction.

4. DYNAMIC ANALYSIS

In this chapter, dynamic behaviour of the system is defined and dynamic analyses are summarized for the 5 MW onshore wind turbine.

4.1. System Dynamics

The wind turbine system has certain elements such as generator, rotor, blades, etc. They have major dynamic effects on the whole system. In the design phase, the frequency of excitation should be taken into consideration to avoid resonance.

To give brief information about the dynamic effects, a Single-Degree-of-Freedom system is considered as shown in Figure 4.1.

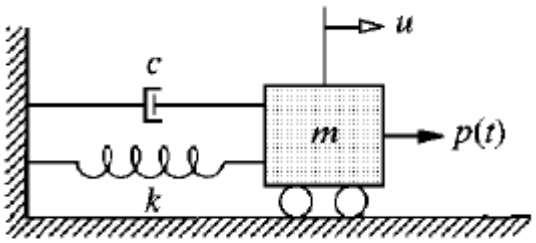

Figure 4.1. SDOF system with mass and damper [34].

p(t) represents the excitation force applied to the mass and there is a viscous damper which has coefficient c. The response of the system is a measure of the frequency of excitation, ω.

The response of the system can be divided into three cases:

- *Quasi-static f< fn*
- *Resonance f=fn*
- *Inertia dominated f>fn*

Where f is excitation frequency in Hz, f_n is natural frequency of the structure [35].

For the first case (quasi-static), the response of the system is almost the same as if the force is static.

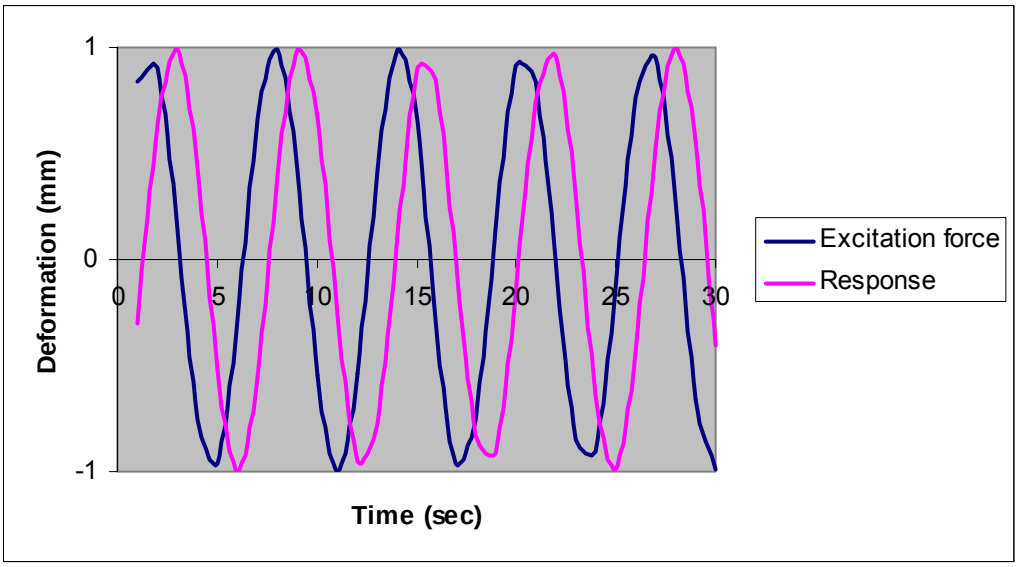

Figure 4.2. Quasi-static response.

For the second case, the frequency of the excitation is close to the system natural frequency. This case is called resonance. The response of the system is much larger than its static response [35].

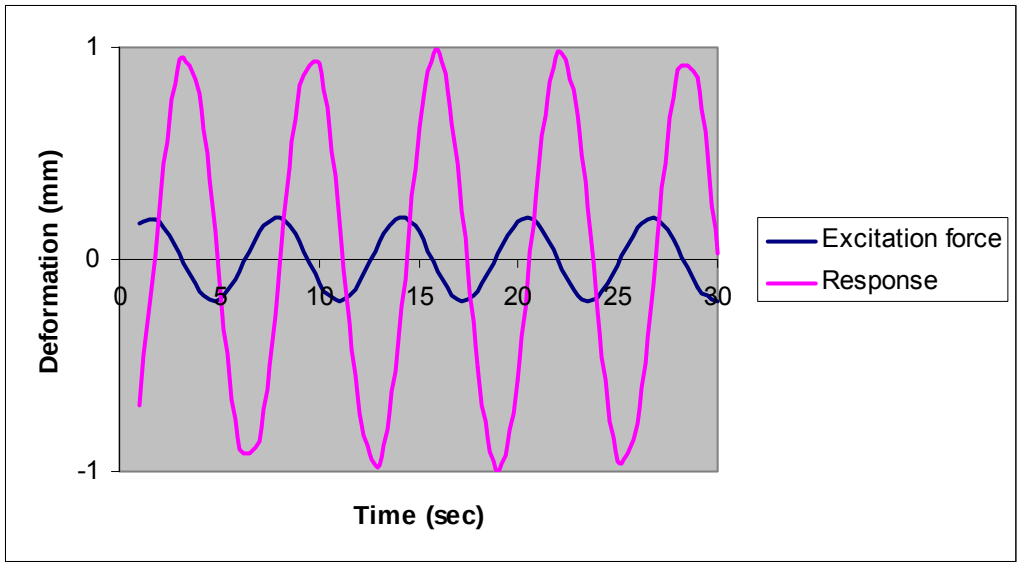

Figure 4.3. Resonant force.

In the last case, the natural frequency of the system is higher than the excitation frequency, then inertia dominates the system. In that case, mass cannot follow the movement [35].

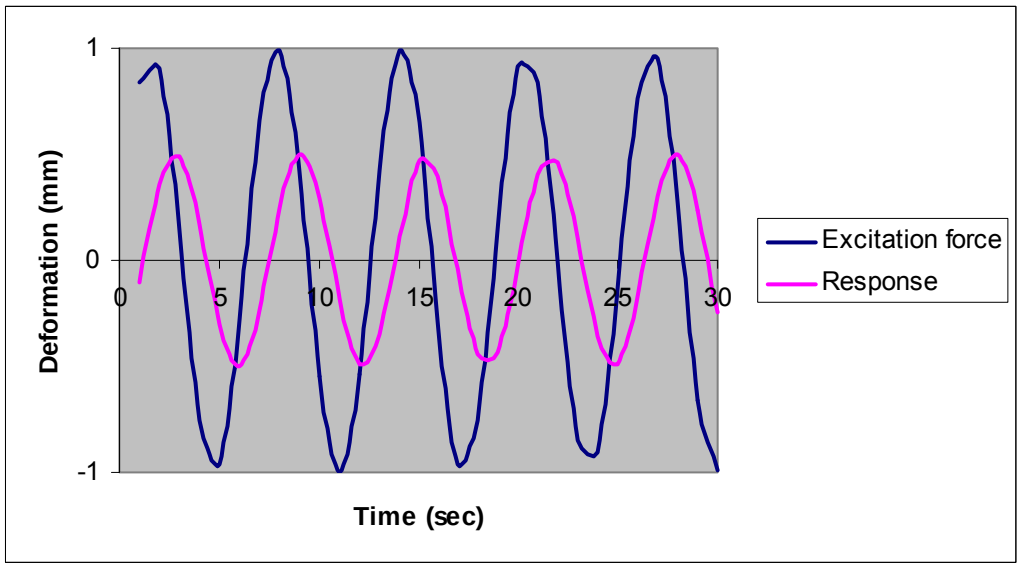

Figure 4.4. Inertia dominated response.

A designer should consider especially the excitation and natural frequencies of a system because the system response can get higher values than expected due to the

resonance effect. Getting the exact values of the response can be decided by the frequency response function as shown in Figure 4.5.

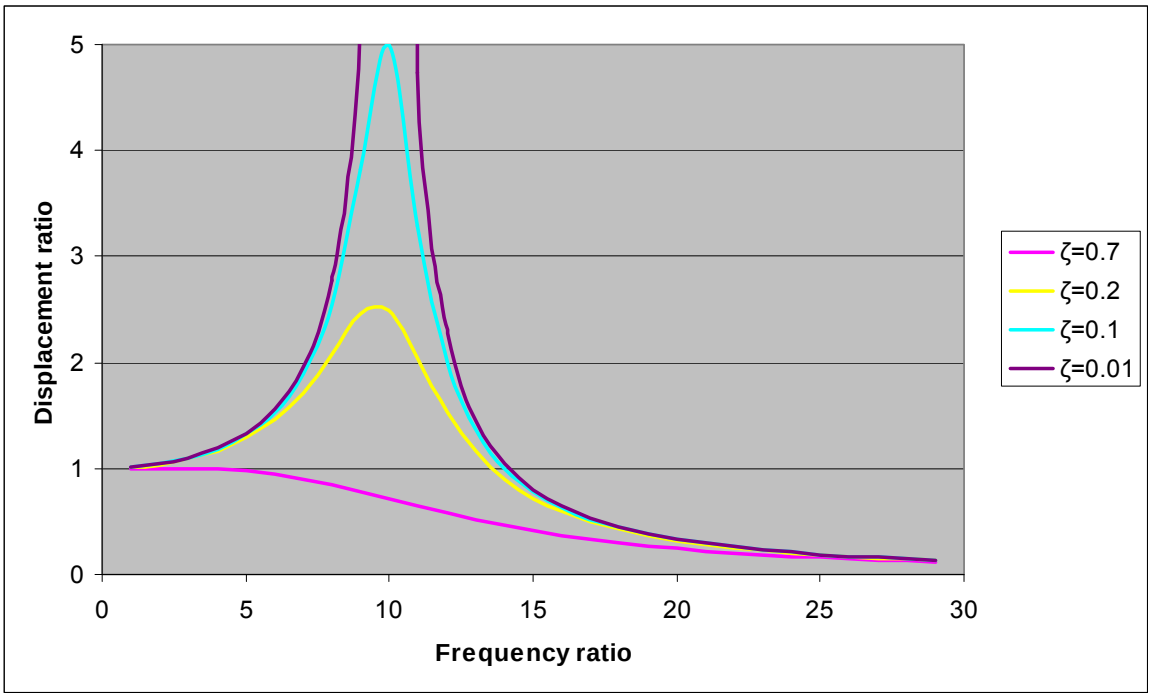

Figure 4.5. Deformation response factor for damped system excited by harmonic force.

R_d value is called the dynamic amplification factor. It is ratio of the dynamic response to the static system response. R_d formulation is:

$$DAF = \frac{u_0}{(u_{st})_0} = \left[\frac{1}{\sqrt{\left[1-(\omega/\omega_n)^2\right]^2 + \left[2\xi(\omega/\omega_n)\right]^2}} \right]$$

4.2. Excitation Generation

In wind turbines, the blades could be manufactured with slightly different masses from each other due to fabrication. The mass imbalance in the blade leads to an excitation force which can be explained by the “excitation generator”.

Vibration generator is a system that leads an excitation in which two or more counter rotating masses force the system to have a harmonic force.

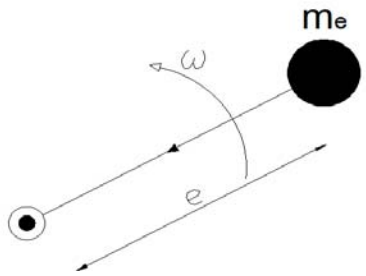

Figure 4.6. A simple form of excitation generator.

In the figure above, there is one mass which have value m_e, excite the system and this force can be transmitted to the system. The amplitude of the harmonic force is proportional to the square of the frequency of excitation [34].

$$p(t) = \left(m_e e \omega^2\right) \sin \omega t$$

In the SAP 2000 “5 sec. period” model, a dynamic force with a sine function is excited to the system at the top of the tower. The response of the system is observed. It can be seen in the Figure 4.8 that the if the excitation frequency coincides with the natural frequency, the response force amplifies.

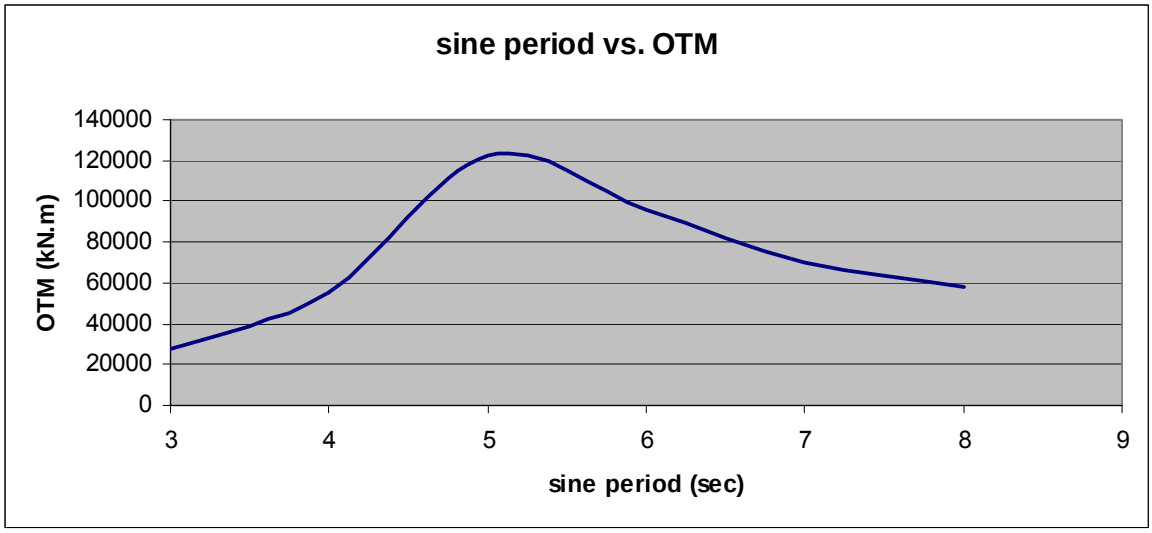

Figure 4.7. sine period vs. OTM graph for the 5 sec. period wind turbine model.

4.3. Campbell Diagram

The fundamental concern for the onshore wind turbine design is to avoid resonance since resonance leads to crucial damage to the whole system or separately for the system units and elements.

Campbell Diagram is a graph that represents a system's response spectrum as the function of its oscillation regime [36]. Figure 4.9 shows the Campbell Diagram which is used in the 5 MW reference turbine design.

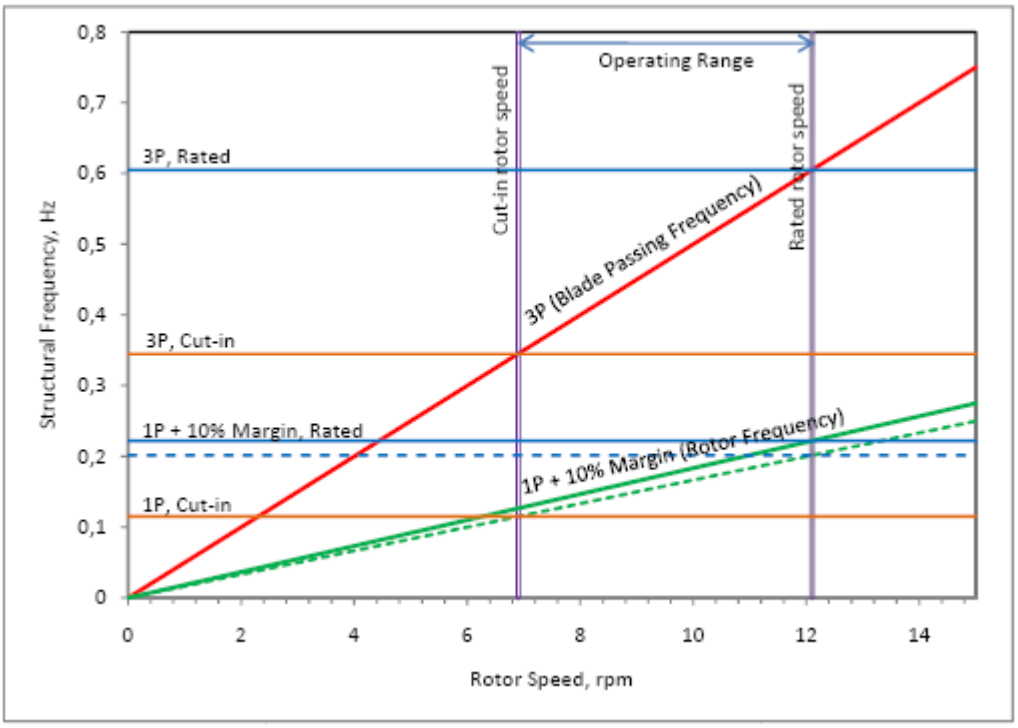

Figure 4.8. Campbell Diagram [29].

In the 5 MW reference turbine, the rotor system has a significant effect on the excitation force to the tower. If we assume that the rotor has a constant rotational speed, this frequency is called the rotor (excitation) frequency. As discussed in the preceding chapter, the blades may have slightly different masses and the center of gravity has an eccentricity. This frequency is called 1P. The second excitation is due to the wind on the tower. When the blade passes in front of the tower, the wind causes a load on the tower where the wind is blocked and vanishes at that moment. For a full circulation of the rotor, this happens Nb (Number of blades) times.

In the operational case, the wind turbine blade rotations are significant when the rotor speed is considered. When the blades start to rotate from rest, their speed and also induced vibration frequency increases. If more output from the turbine is desired, the blades rotate faster and the rotational speed leads to the operational frequency getting closer to the system natural frequency, which can lead resonant amplification. This situation can cause higher dynamic forces which can lead to damage to the structure. Even if these forces do not reach the elastic-limit or the structural strength capacity, fatigue

damage can occur. Therefore, in the design phase, the rotor speed turns out to be important [3].

Figure 4.9 shows that the onshore wind turbine has 6.9 rpm cut in rotor speed and 12.1 rpm rated rotor speed. The main goal is to stay away from resonance. For that purpose, the structure should be designed out of the zones of 1P and 3P. Figure 4.10 shows that there are three possible zones. The system can be very stiff with a frequency greater than 3P (stiff-stiff), with a natural frequency of between 1P and 3P (soft-stiff) or a very soft structure with a frequency lower than 1P (soft-soft) [29].

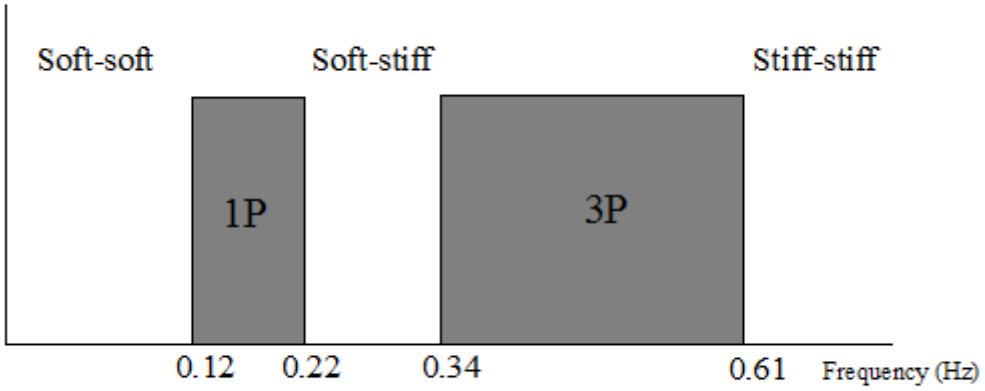

Figure 4.9. Frequency intervals of the 5 MW wind turbine [35].

The natural frequency of the onshore wind turbine should be chosen between 0.22 and 0.34 Hz that is equal to 4.55 sec and 2.94 sec periods. The designer can choose a frequency closer to 0.22 Hz for economic reasons.

4.4. Dynamic Analysis of the Model

In this chapter, the structure is analyzed in terms of base shears and overturning moments according to the wind data which are created by the TurbSim code. In the TurbSim code, 11.4 m/s mean wind speed stochastic data are created randomly for 10

different seeds. These seeds display different stochastic characteristics; however, all of them have the same mean wind speed, 11.4 m/sec. Figure 4.11 shows an example wind speed time history used in the analyses.

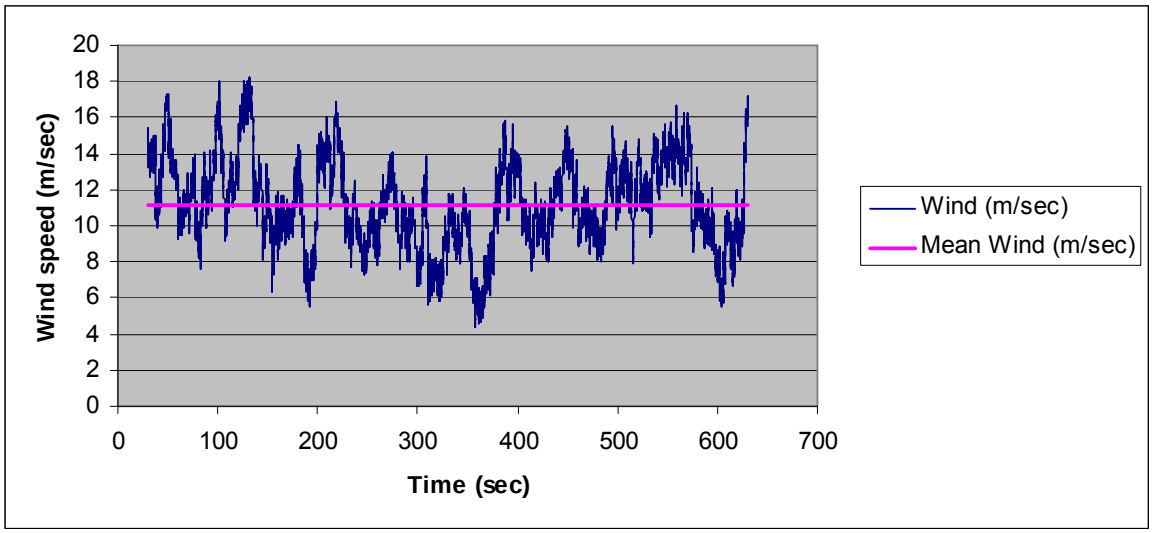

Figure 4.10. Stochastic and Mean Wind Speeds for T=4.69 sec. (seed 1).

Dynamic analysis of the structure is carried out for 600 seconds. At the end of analysis for each seed, time history results and their maximum values are obtained.

In Figure 4.12 base shear time history and in Figure 4.13 over-turning moment time history obtained for the first seed are plotted.

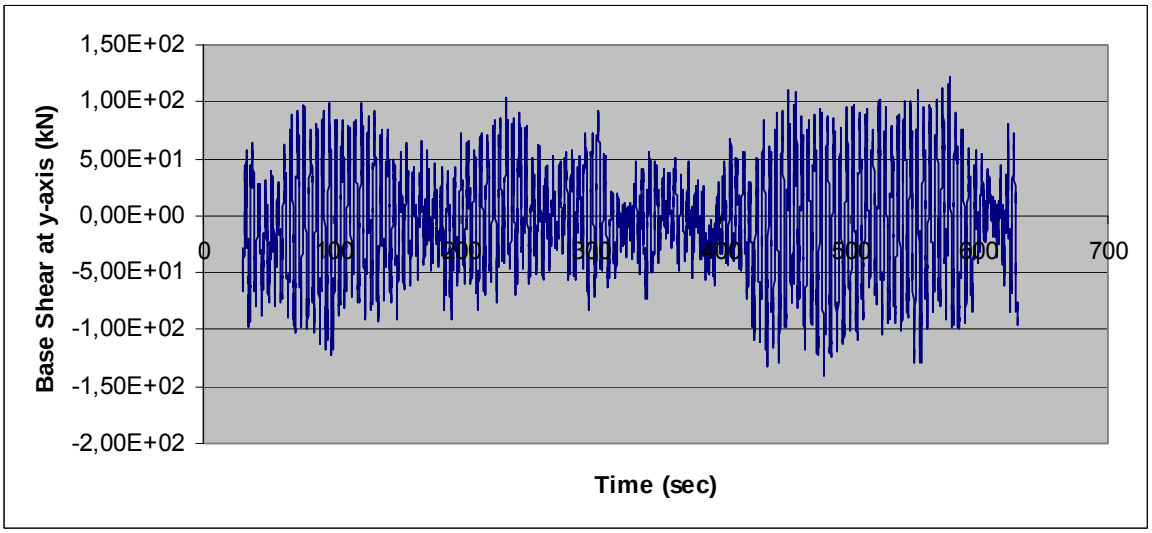

Figure 4.11. Stochastic Tower Base Shears for T=4.69 sec. (seed 1).

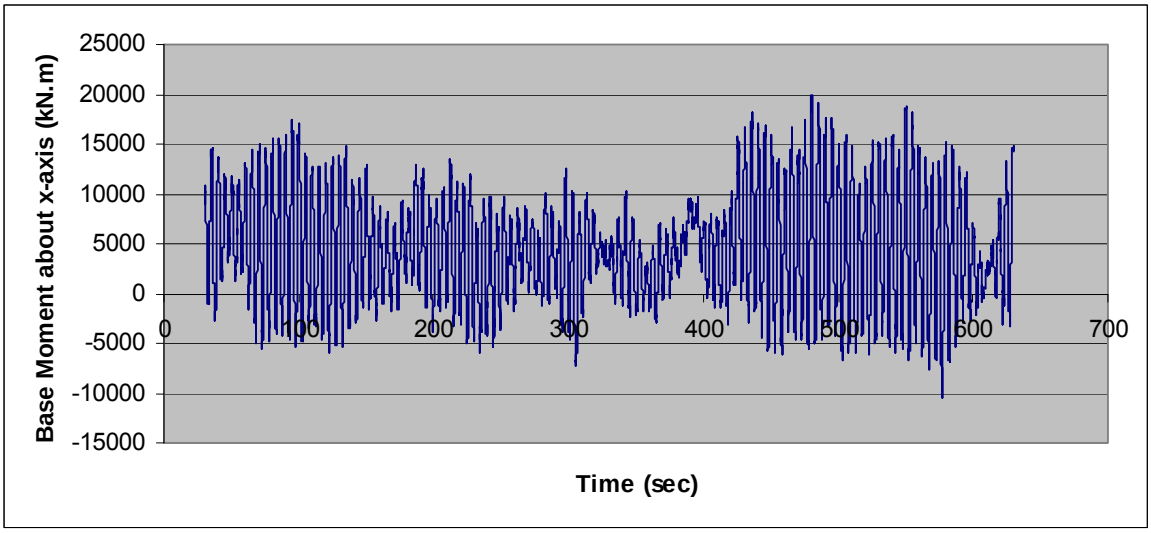

Figure 4.12. Stochastic Overturning Moments for T=4.69 sec. (seed 1).

Due to the variance of each wind speed and OTM values at different seeds, sensitivity analysis is carried out to get optimum values to use in the fatigue analysis. In Figure 4.14 and Figure 4.15 maximum wind speed and maximum OTM values are plotted for 10 different seeds of resonance case. Mean of the maximum BS & OTM values are obtained after each seed. Figure 4.16 shows that after 10 seeds convergence is achieved.

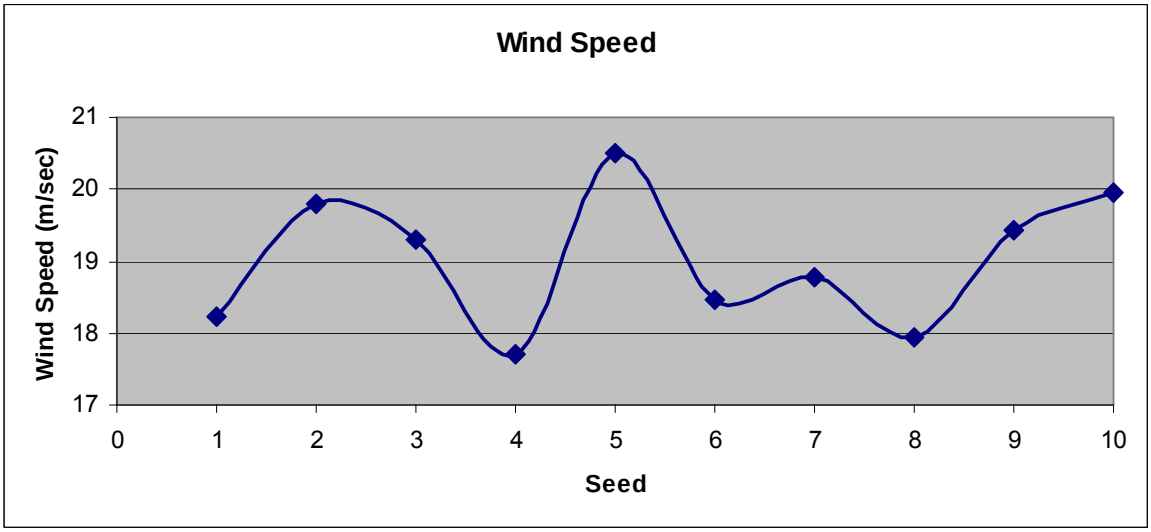

Figure 4.13. Maximum Wind speed values graph for 10 seeds of resonance case.

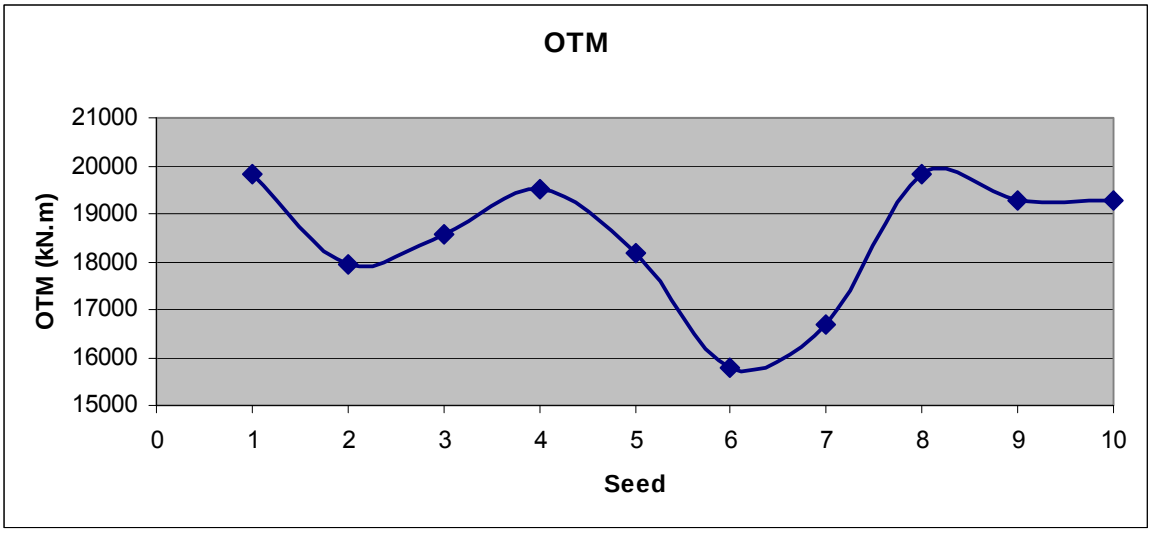

Figure 4.14. Maximum OTM values graph for 10 seeds of resonance case.

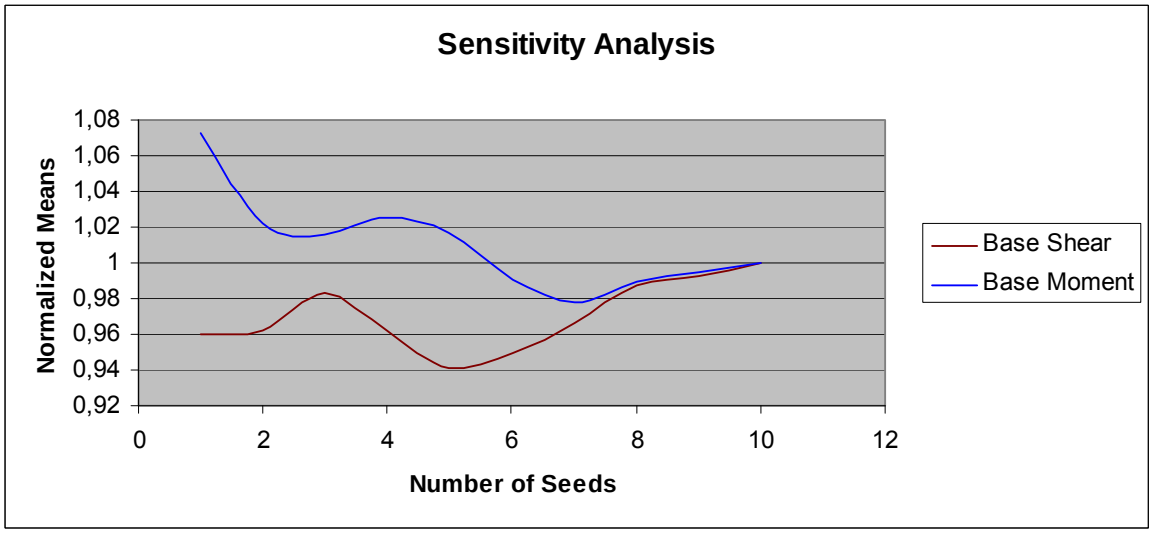

Figure 4.15. Sensitivity analysis for 10 seeds at period of 4.69 sec.

In this thesis, the structure is analyzed considering its resonance behaviour in the perpendicular direction of the wind. The results of the response values for 8 different models with different periods are tabulated below.

Table 4.1 Base Moment and Base Shear Results for 8 different models.

Period (sec)	Penetration depth (m)	Base Shear (kN)	Base Moment (kN.m)
3.9	-15	76	11673
4.15	-20	**91**	**11838**
4.36	-24	86	13824
4.52	-27	99	14127
4.69	-30	**128**	**14648**
5.16	-35	120	13821
6.08	-50	94	10567
7.10	-65	86	10929

Figure 4.17 and Figure 4.18 show that the maximum base shear and over turning moment values occurs in the model with the natural period of 4.69 seconds. The model with this period values lies within 1P region of Campbell Diagram; therefore, it represents "in-resonance" case.

In Figure 3.16 of the previous chapter, it was shown that natural period of the structure changes with the change in soil stiffness. Based on the this figure, if the subgrade soil reaction modulus value is approximately 15000 kN/m^3, the structural period turns out to be 4.15 seconds which represents the "out-of-resonance" case.

On the other hand, if the subgrade soil reaction modulus value is approximately 7500 kN/m^3, the structural period turns out to be 4.69 seconds which represents the "in-resonance" case.

With an approximate value of 4000 kN/m^3 subgrade soil reaction value that corresponds the 6.08 sec. case, the base shear and OTM values return proximity of the "out-of-resonance" case again. It can be observed that the soil stiffness affects the dynamic response of the structure seriously.

In the fatigue analysis, two models with different structural periods are considered to study the resonance effect. "4.69 sec" and "4.15 sec" periods are chosen to compare "in-resonance" and "out-of-resonance" loads on the critical joints on the tower.

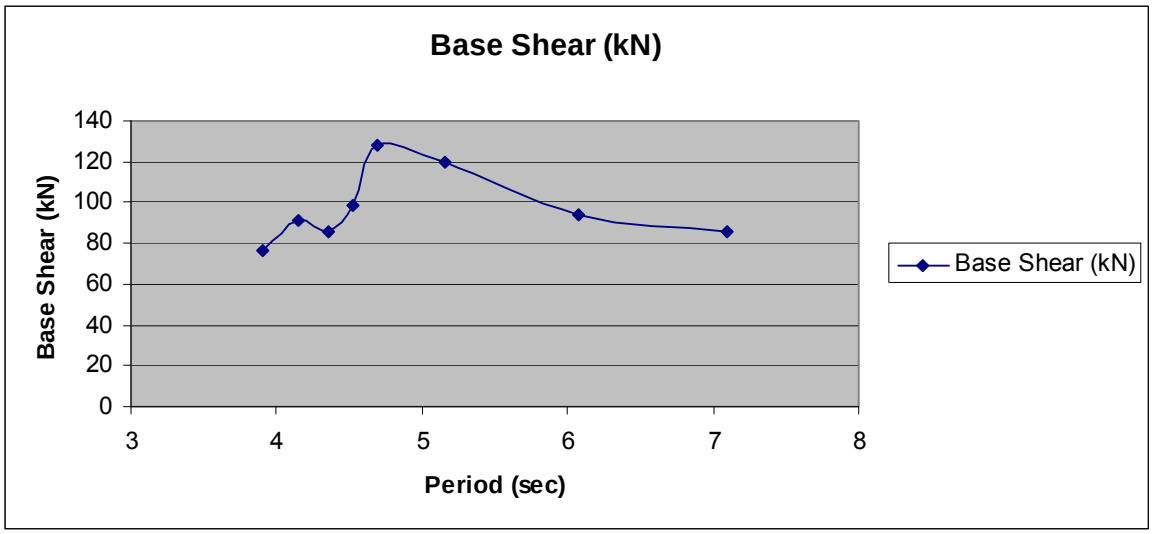

Figure 4.16. Base Shear Diagram.

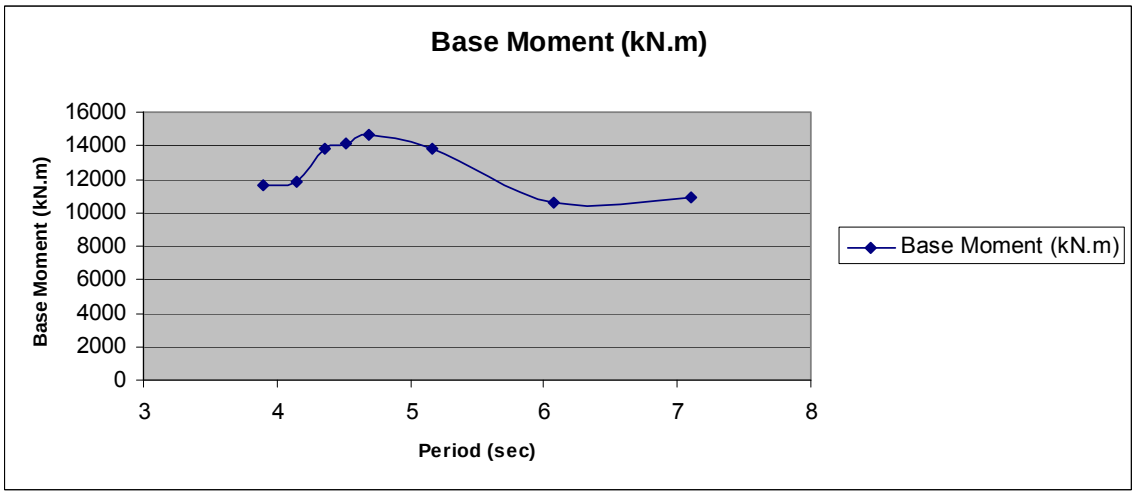

Figure 4.17. OTM Diagram.

4.5. Strength Check

In this part, the strength analyses of the wind turbine are performed. The across-wind values are taken into consideration because they result in higher demand values. Steel structure design checks are made according to API RP-2A [37]. Design checks are commonly carried out for bending and buckling. In this part, the across-wind values are considered because of their critical ranges. Allowable bending stress and allowable shear stresses for cylindrical members can be computed by the following equations .

First of all, the elastic local buckling should be checked:

If 300>D/t>0.6 and t≥6 mm the elastic local buckling stress F_{xe};

$$F_{xe} = \frac{2CEt}{D}$$

Where C is critical elastic buckling taken as 0.6, D is outside diameter in m, T is wall thickness in m.

F_{xe}= 1134 MPa

The inelastic buckling stress for D/t≤60 Fxc;

$$F_{xc} = F_y \times \left[1.64 - 0.23(D/t)^{1/4}\right] \leq F_{xe}$$

F_{xc}= $250 \times \left[1.64 - 0.23(6/0.027)^{1/4}\right]$ = 188 MPa

$F_{y,new}$=Smaller (F_{xe}; F_{xc})= 188 MPa

$$C_c = \left(\frac{2\pi^2 E}{F_y}\right)^{1/2}$$

Where E is Young's Modulus of Elasticity in MPa, K is effective length factor, l is unbraced length in m, r is radius of gyration in m.

Cc= 148.5

Where F_y is yield strength in MPa taken as 250 MPa, E isYoung's Modulus of Elasticity in MPa taken as 210000 MPa, D is outside diameter in m taken as 6.00 m, t is wall thickness in m taken as 0.027 m, K is effective length factor taken as 2, l is unbraced length in m that for the period 4.69 sec taken as 117.6 m, r is radius of gyration in m, C is critical elastic buckling coefficient.

$$F_a = \frac{\left[1 - \frac{(Kl/r)^2}{2C_c^2}\right]F_y}{5/3 + \frac{3(Kl/r)}{8C_c} - \frac{(Kl/r)^3}{8C_c^3}} \text{ for } Kl/r < C_c$$

F_a= 102.1 MPa

For bending;

$$F_b = \left[0.72 - 0.58\frac{F_y D}{Et}\right]F_y \text{ for } \frac{3000}{F_y} < \frac{D}{t} \le 300$$

F_b= 141.64 MPa

$$F_v = 0.4 \times F_y = 0.4 \times 250 = 100 \text{ MPa}$$

For maximum shear stress,

$$f_v = \frac{V_{tr}}{0.5 \times A}$$

Where V_{tr} is transverse shear force in MN, A is the cross sectional area in m^2.

$$f_v = \frac{0.992}{0.5 \times 0.507} = 3.913\,\text{MPa} < 100\ \text{MPa}$$

For compression strength check $f_a < F_a$ should be satisfied;

$$f_a = \frac{\text{Total Weight}}{\text{Area}} = \frac{6.157}{0.507} = 12.14\ \text{MPa} < 102.1\ \text{MPa}$$

Finally, combined bending and compression should be checked:

$\frac{f_a}{0.6F_y} + \frac{\sqrt{f_{bx}^2 + f_{by}^2}}{F_b} \le 1.0$ should be satisfied that:

F_{bx} and f_{by} are computed bending tensile stresses ; $f_b = \frac{M \times y}{I}$

I is the inertia of the member section

$$I = \pi\left(d_{out}^4 - d_{in}^4\right)/64\ \text{m}^4$$

$$f_b = \frac{M \times y}{I} = \frac{83318 \times 3}{2.26} = 110599\,\text{kN/m2} = 110.6\ \text{MPa}$$

$$\frac{f_a}{0.6F_y} + \frac{\sqrt{f_{bx}^2 + f_{by}^2}}{F_b} = 0.86 < 1.00$$

With respect to the strength analysis, the tower is on the safe side according to the API RP 2A code requirements. 86 % of the tower bearing capacity under combined axial and bending loading is used in the most critical case.

5. FATIGUE ANALYSIS

In this chapter, fatigue life analysis for the most critical parts of the wind turbine is performed. In the onshore wind turbine system, one of the most critical parts are the bolts. In this chapter, the bolts are analyzed for the “in-resonance” and “out-of-resonance” cases. Consequently, the effect of the resonance in the fatigue life of the bolts are observed.

5.1. Fatigue Definiton

Fatigue is a progressive and localized structural damage which occurs in a cyclic loading [38]. Fatigue failure generally occurs under the yield limit stress.

If a material is subjected to a cyclic load, a fatigue crack nucleus may be initiated on a microscopic scale which is followed by macroscopic crack growth. To understand the fatigue mechanism, it is essential to consider various technical conditions which affect fatigue life and crack growth, such as material surface properties, residual stress and environmental effects [39].

Fatigue life can be evaluated usually in two phases; the crack initiation phase and the crack growth phase. The initiation period is assumed to include microcrack growth; however, the fatigue cracks are still too small to be visible to the unaided eye. In the second phase, crack growth continues until the failure occurs [39].

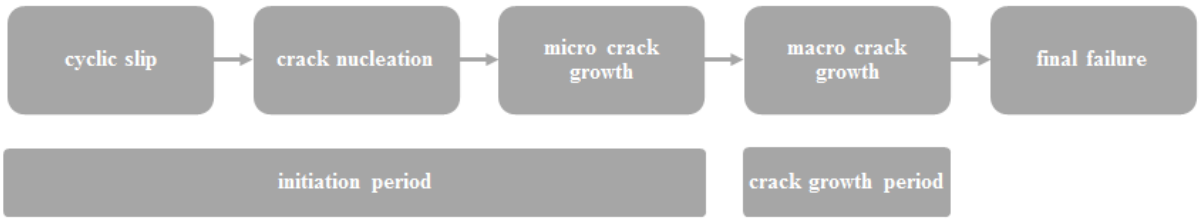

Figure 5.1. Different stages of the fatigue life and relevant factors [39].

5.1.1. Crack initiation

Fatigue crack initiation and crack growth are the consequences of cyclic slip in the slip bands. It shows cyclic plastic deformation as a result of moving dislocations. Fatigue occurs at stress amplitudes below the yield limit stress. At a low stress level, plastic deformation is restricted to a small number of grains. This micro-plasticity can occur more easily on the surface of the material because the other side of the grain is surrounded by the material. Therefore, plastic deformation occurs at lower stress levels on the surface material due to the environmental effects [39].

Cyclic slip needs cyclic shear stress. On the microscale, the shear stress is not distributed homogenously in the material. The shear stress on crystallographic slip planes differs from grain to grain depending on the shape and size of the grains [39].

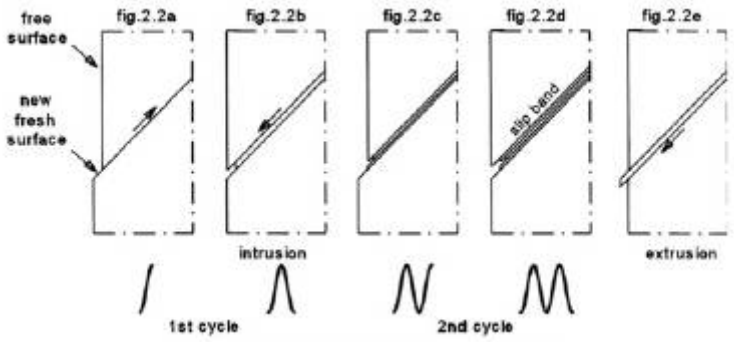

Figure 5.2. Cyclic slip stages [39].

5.1.2. Crack growth

The microcracks contribute to an inhomogenous stress distribution on a micro level. Furthermore, if the crack growth continues into the material in some adjacent grains, the constraint on slip displacements will increase due to the presence of the neighbouring grains. Therefore, it will become increasingly difficult to accommodate the slip displacements by a single slip system only. It should occur on slip planes in different directions. The microcrack growth direction will deviate from the initial slip band

orientation. Because microcrack growth depends on the plastic cycling, barriers to slip can imply a threshold for crack growth [39].

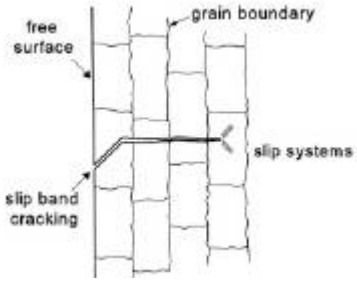

Figure 5.3. A simple figure of microcrack [39].

Due to the crack front phenomenon, the crack cannot grow in each grain in an arbitrary direction or at any growth rate independent of crack growth in the adjacent grains [39].

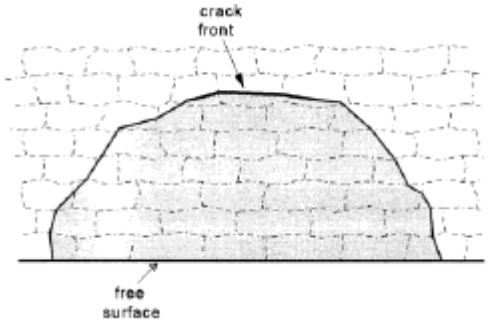

Figure 5.4. Crack with crack front passing through the grains [39].

This continuing crack formation prevents large gradients of the crack growth rate along the crack front. As a result, as such a number of grains along the crack gets sufficiently larger, it leads to less continuity along the crack front. The crack speed depends on the crack growth resistance of the material. Therefore, the crack growth phenomenon depends on the bulk material property [39].

5.1.3. S-N curve

To understand the fatigue life assessment in the design process, an empirical design methodology must be used. Firstly, an S-N curve should be generated for a material that is used in a structural detail or connection. Firstly, a testing specimen is fixed using testing equipment and sinusoidal stress variations are applied to the material. By counting the number of cycles that is required to fail under the applied stress range, a single point on the failure envelope can be determined. This process is applied for the different stress levels and therefore, the fatigue loading can be expressed by the stress range by a diagram which is called an S-N curve or Wöhler curve [30].

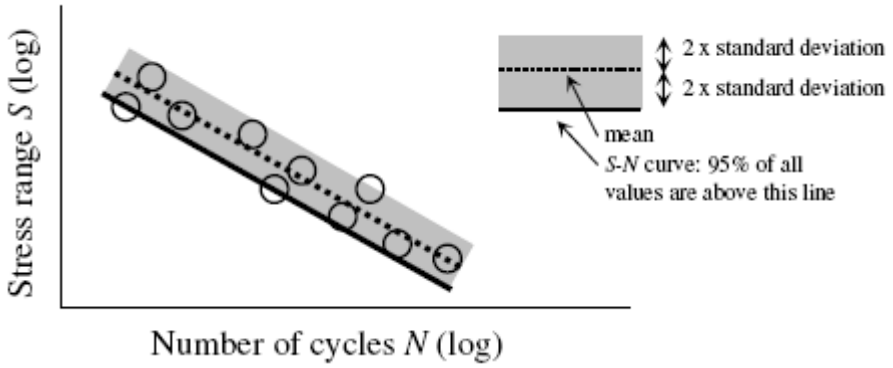

Figure 5.5. Failure point at certain stress ranges in failure cycles and the corresponding S-N curve [30].

The S-N diagram plots nominal stress amplitude (S) versus cycles to failure (N). There are numerous tests to produce the required data for a proper S-N curve [40].

An S-N curve can be generated on a log-log scale diagram by a power relationship as:

$$N_1 = N_2\left(\frac{S_1}{S_2}\right)^{1/b}$$

Where b is slope of the line (refferred as Basquin slope), S_1 and S_2 are stress values at point 1 and 2, N_1 and N_2 are cycle numbers at point 1 and 2.

$$b = \frac{-(\log S_1 - \log S_2)}{\log N_2 - \log N_1}$$

Which gives a graph;

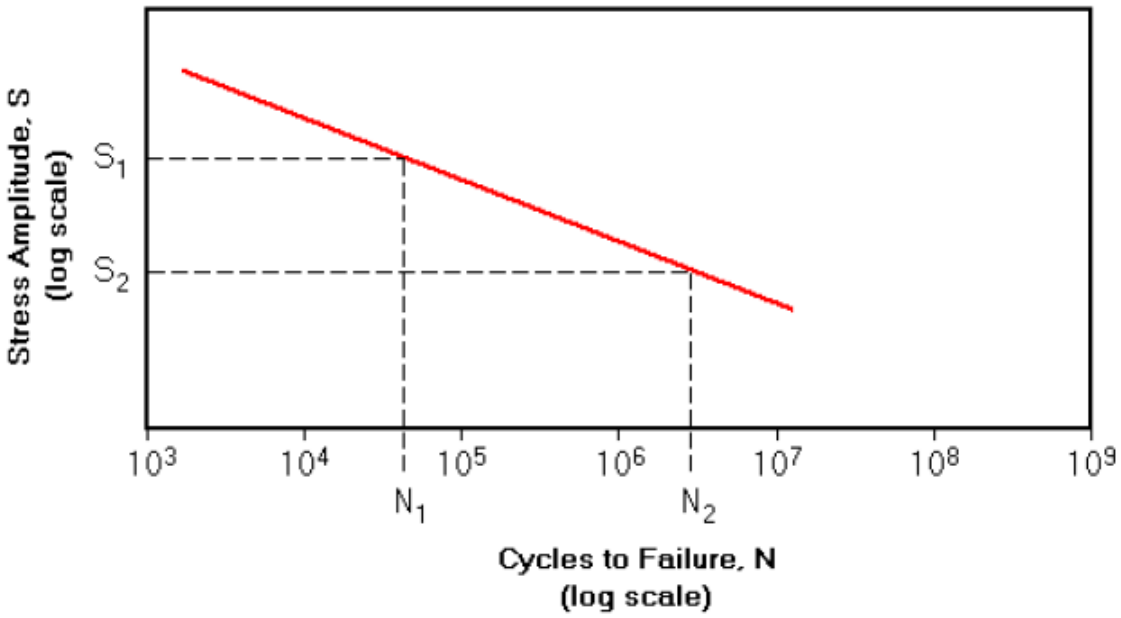

Figure 5.6. Idealized S-N Curve [40].

5.1.4. Miner's Rule

Miner's rule is one of the most commonly used methods to calculate the fatigue damage in a material. This rule was popularised by M. A. Miner in 1945.

Miner's rule or the Palmgren-Miner linear damage hypothesis states that the total damage equals the sum of the n_i (actual cycle number at i^{th} stress) over N_i (capacity of cycle number at i^{th} stress).

For highly irregular variations in stress histories, it is difficult to isolate each stress cycle and to group them into bins. A number of different methods were proposed to count the stress cycles. The most known procedure is “rainflow cycle counting” which is developed by Prof. T. Endo and his colleagues. In this procedure, peaks, valleys and time dependent stress reversals are crucial criteria for counting stress cycles. In this thesis, rainflow counting method is not used. Stress cycles are counted according to their number of occurrences in the given stress history. Peaks and valleys or any other criteria are not taken into consideration [42].

$$\sum_{i=1}^{k} \frac{n_i}{N_i}$$

Where n_i is actual cycles in i^{th} stress range, N_i is cycle capacity of the material in i^{th} stress range, C is failure capacity which assumed to be 1.

If the sum of the n_i/N_i gets 1, the system fails due to the fatigue damage.

Fatigue calculation for variable stress ranges in time domain can be summarized as shown in Figure 5.7.

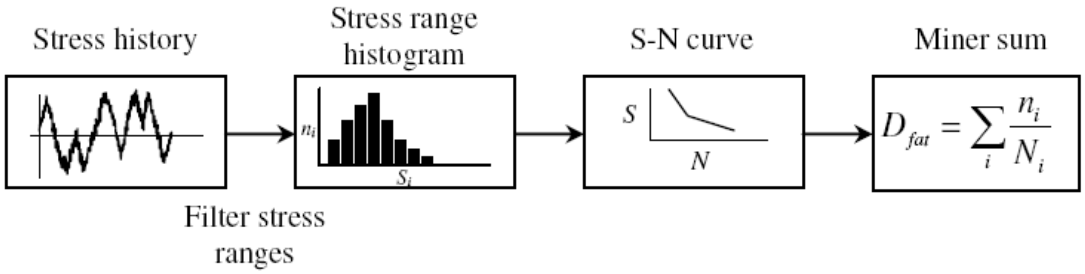

Figure 5.7. Flowchart of fatigue calculation [30].

5.2. Fatigue Life Analysis

In this part, fatigue life analyses of the “in-resonance” and “out-of-resonance” cases are conducted. Figure 5.8 shows the S/N curve for High Strength Bolts that is used in the analyses.

In the thesis, fatigue life analyses are conducted according to some assumptions:

- Prestress and mean stress are not included in fatigue calculations.
- Shear stress is neglected due to its small value.
- Moment of inertia at that flange is assumed to be identical material (tower steel) and uniform.
- Only the axial dead load and bending moment are taken into consideration.

The flange of the section is designed as the bolts bear the axial dead load and bending moments.

Stress formulation is:

$$\sigma = \frac{N}{A} \pm \frac{My}{I}$$

Where N is axial load in kN (F= 6157 kN), A is area of the section, m^2 (A=0.507 m^2), M is moment about the x-axis in kN.m, y is location of the calculated stress point in m (y= 3.00 m), I is area moment of inertia of the section in m^4 (I=2.26 m^4).

Figure 5.8 shows S/N curve for High Strength bolts.

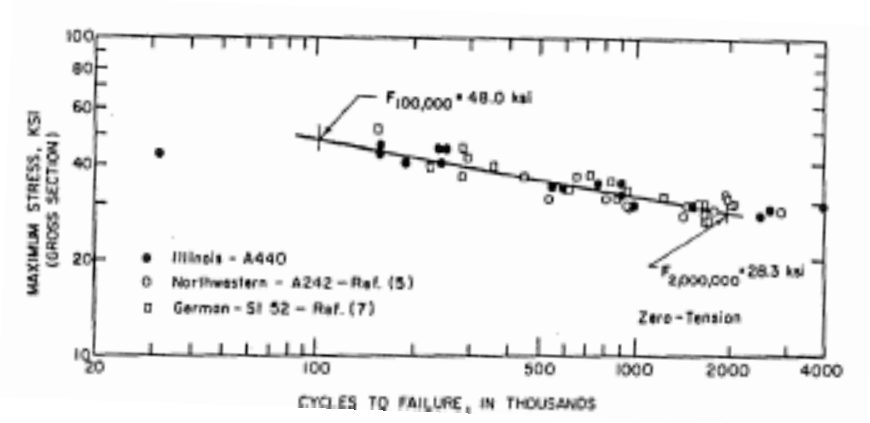

Figure 5.8. S/N curve for High Strength Bolts [41].

Figure 5.9 shows joint locations for a wind turbine tower part.

Figure 5.9. Wind turbine joint locations.

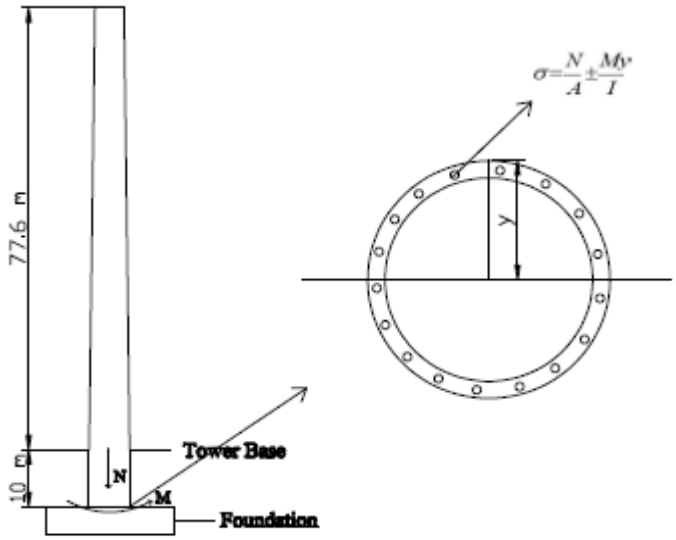

Figure 5.10. Representation for the bolts.

Figure 5.10 shows a representation for the location of the bolts and the stress formulation that is used in the analyses.

5.2.1. Analysis for 4.15 sec case

Figure 5.11 shows stress-time history graph for the first seed of "out-of-resonance" case.

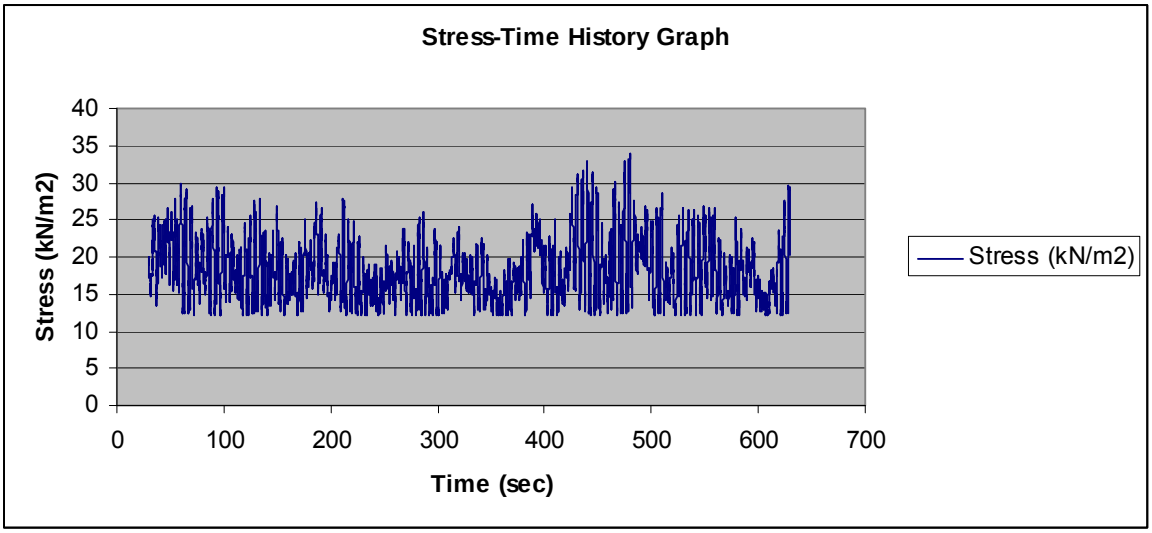

Figure 5.11. Stress-time history graph for 4.15 sec (seed 1).

In the Table 5.1, average fatigue life of the bolts for 4.15 sec. case is displayed. The probability of occurences are found based on Miner's Rule. Fatigue life is obtained as 1/Probability of occurence.

The average life of the bolt for 4.15 sec. case is 1205.796 years.

Table 5.1. Fatigue Life Data for 4.15 sec case.

Seeds	Probability of occurences	Years
1	4.33192E-08	1098.005
2	4.11587E-08	1155.642
3	4.11904E-08	1154.752
4	4.23673E-08	1122.675
5	3.85081E-08	1235.188
6	4.14620E-08	1147.188
7	3.65836E-08	1300.164
8	3.77519E-08	1259.929
9	3.59893E-08	1321.635
10	3.76666E-08	1262.781
	AVERAGE	*1205.796*

5.2.2. Analysis for 4.69 sec case

Figure 5.13 shows stress-time history graph for the first seed of "in-resonance" case.

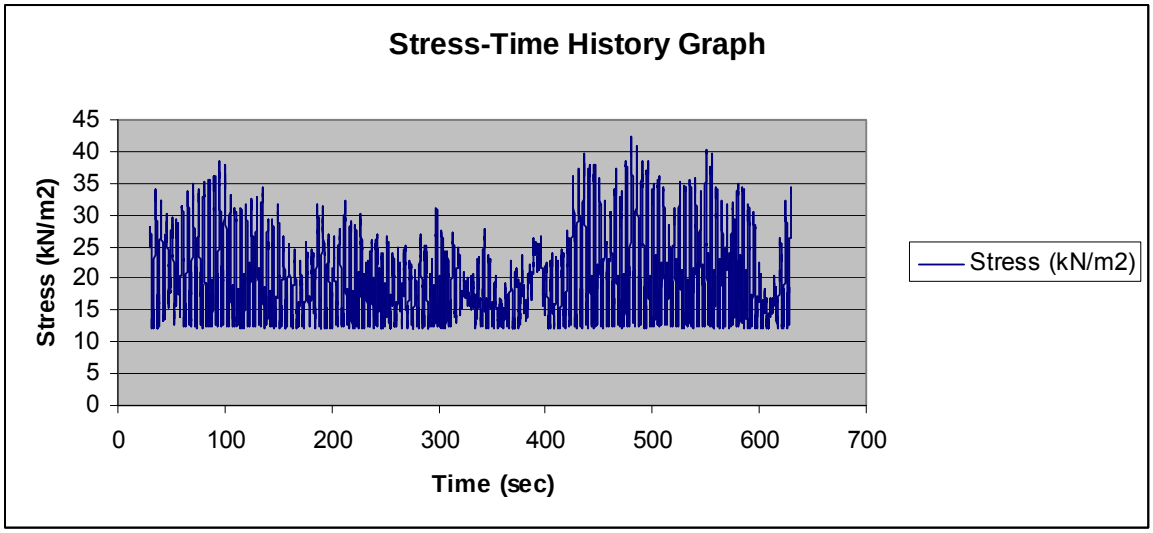

Figure 5.12. Stress-time history graph for 4.69 sec (seed 1).

Table 5.2 shows the average fatigue life of the bolts for the "in-resonance" case. For the resonance case, the life of the bolt is 429.204 years.

Table 5.2. Fatigue Life Data for 4.69 sec case.

Seeds	Probability of occurence	Years
1	1.20354E-07	395.206
2	1.14904E-07	413.950
3	1.19217E-07	398.977
4	1.31613E-07	361.398
5	1.09877E-07	432.892
6	1.10830E-07	429.168
7	1.02141E-07	465.674
8	1.16471E-07	408.383
9	8.72955E-08	544.870
10	1.07728E-07	441.526
	AVERAGE	*429.204*

According to the 10 minutes analysis, the fatigue lives are found 1280.169 and 454.843 years, for “out-of resonance” and “in-resonance” cases respectively. Extending the analysis time affects the fatigue life results of the material, significantly.

5.2.3. Probability of Failure

In the probability of failure calculation, an exponential failure distribution method is used. The formulation is:

$$F(t) = \int_0^t \lambda e^{-\lambda\tau} d\tau = 1 - e^{-\lambda t}$$

Where λ is failure rate and t is time to fail.

For the period 4.15 sec;
$\lambda = 8.29 \times 10^{-4}$.

For the period 4.69 sec;
$\lambda = 2.33 \times 10^{-3}$.

For the time interval for t =100 years failure probabilities are;
for 4.15 sec: F(t)= 0.0796 = 8 %
for 4.69 sec: F(t)= 0.2079 = 21 %

This result shows that in the resonance situation, the probability of the fatigue failure occurence is approximately three times the normal condition.

6. CONCLUSION

All through the study, several subjects about the onshore wind turbines are presented. The conclusions can be stated as below.

- The constant wind speed should not be used due to the stochastic nature of the wind that amplifies the response of the structure. Constant wind speed does not give accurate results in that manner.Due to the stochastic nature of the wind, base shear and overturning moments can be altered for each simulation; therefore, sufficient number of seed should be used.
- In the foundation modelling, the stiffness of the soil affects the system natural frequency.
- Due to soil uncertainty, the frequency value may fall into 1P range as a consequence resonance may happen. This situation is significant for the perpendicular to wind direction.
- Fatigue analysis results showed that due to resonance fatigue life of the joints is about one third for the “in-resonance” case compared to “out-of-resonance” case. Also, it is seen that the simulation time length significantly influences the fatigue occurrence probability calculations.

Further studies;

- The structures such as truss type, can be investigated for the optimum design concept.
- Soil behaviour can be taken into consideration in detail for further studies.
- Fatigue life of the bolts and/or rods can be assessed by detailed finite element analyses to for more realistic evaluation of maximum stress values.
- In the fatigue analysis, different cycle counting methods can be performed to determine the fatigue life estimation.

REFERENCES

1. Zaaijer, M.B., *Foundation Modelling to Assess Dynamic Behaviour of Offshore Wind Turbines*, Applied Ocean Research, Vol. 28, pp. 45-57, 2006.

2. Kühn, M., *Soft or Stiff – A Fundamental Question for Designers of Offshore Wind Energy Converters*, European Wind Energy Conference EWEC 97, Dublin, Ireland, 1997.

3. Bhattacharya S., S., Adhikari, *Experimental Validation of Soil-Structure Interaction of Offshore Wind Turbines*, Soil Dynamics and Earthquake Engineering, Vol. 31, pp. 805-816, UK, 2011.

4. AlHamaydeh, M. and Hussain, S., *Optimized Frequency-Based Foundation Design for Wind Turbine Towers Utilizing Soil-Structure Interaction*, Journal of Franklin Institute, Vol. 348, Issue 7, pp. 1470-1487, 2011.

5. Ozdemir, Y.I., *Development of a Higher Order Finite Element on a Winkler Foundation*, Finite Elements in Analysis and Design, Vol. 48, pp. 1400-1408, Turkey, 2012.

6. Huang, M.H. and Thambiratnam, D.P., *Analysis of Plate Resting on Elastic Supports and Elastic Foundation by Finite Strip Method*, Computers and Structures, Vol. 79, pp. 2547-2557, Australia, 2001.

7. Daloglu, A.T., and Vallabhan, C.V.G., *Values of k for Slab on Winkler Foundation*, Journal of Geotechnical and Geoenvironmental Engineering, Vol. 126, No. 5, pp. 463-471, 2000.

8. Kim, Y.M. and You K.P., *Dynamic Responses of a Tapered Tall Building to Wind Loads*, Journal of Wind Engineering and Industrial Aerodynamics, Vol. 90, pp. 1771-1782, South Korea.

9. Maalawi, K.Y., *A Model for Yawing Dynamic Optimization of a Wind Turbine Structure*, International Journal of Mechanical Sciences, Vol. 49, pp. 1130-1138, Egypt, 2007.

10. Veers, P.S. and Winterstein, S.R., *Application of Measured Loads to Wind Turbine Fatigue and Reliability Analysis*, ASME Wind Energy Symposium – Held in conjuction with the AIAA Aerospace Sciences Meeting, Reno, Nevada, USA, January 6-9 1997.

11. Cho, S.S., Chang, H., Lee, K.W., *Dependence of Fatigue Limit of High-Tension Bolts On Mean Stress and Ultimate Tensile Strength*, International Journal of Automotive Technology, Vol. 10, No.4, pp. 475-479, Korea, 2009.

12. J.D. Holmes, *Fatigue Life Under Along-Wind Loading – Closed-Form Solutions*, Engineering Structures, Vol. 24, pp. 109-114, Australia, 2002.

13. *What Is Wind?*, RenewableUK, http://www.bwea.com/edu/wind.html, accessed at January 2010.

14. *History of Wind Power Development*, Dodge, D.M., http://www.telosnet.com, accessed at January 2010.

15. *History of Wind Power*, Wikipedia, http://en.wikipedia.org/wiki/History_of_wind_power, accessed at May 2012.

16. *Panemone Windmill*, Wikipedia, http://en.wikipedia.org/wiki/Panemone_windmill, accessed at July 2012.

17. Tong W., *Wind Power Generation and Wind Turbine Design*, WIT Press, 2010.

18. *Renewable Energy*, Wikipedia, http://en.wikipedia.org/wiki/Renewable_energy, accessed at July 2012.

19. *Renewables 2011-Global Status Report*, Ren21, http://www.ren21.net/Portals/97/documents/GSR/REN21_GSR2011.pdf, accessed at July 2011.

20. *GWEC Global Wind Statistics 2010*, Global Wind Energy Council, http://www.gwec.net/fileadmin/documents/Publications/GWEC_PRstats_02-02-2011_final.pdf, accessed at January 2011.

21. *10 Years of Electricity Production Capacity Projection of Turkey, 2011-2020*, Republic of Turkey Energy Market Regulatory Authority (EMRA), http://www.epdk.org.tr/documents/elektrik/rapor_yayin/Elk_Yayin_Uretim_Kapasite_Projeksiyonu_2011_2020.pdf, accessed at November 2011.

22. *Wind Speed Map of Turkey for the Height of 50 m*, Turkish State Meteorological Service, http://www.mgm.gov.tr/arastirma/yenilenebilir-enerji.aspx?s=ruzgaratlasi, accessed at January 2012.

23. *5 MW Onshore Wind Turbine Figure*, Global Greenhouse Waming, http://www.global-greenhouse-warming.com/largest-wind-turbine.html, accessed at May 2008.

24. *Rotor-Nacelle Assembly Figure*, National Renewable Energy Laboratory, http://www.nrel.gov/news/features/feature_detail.cfm/feature_id=1814?print, accessed at March 2012.

25. Jonkman, B.J., *TurbSim User's Guide (Version 1.50)*, NREL/TP-500-46198, National Renewable Energy Laboratory, accessed at September 2009.

26. *Comparative Study of OWTG Standards*, MMI Project No. MMW528, MMI Engineering, USA, 2009.

27. *Normal Distribution*, Wikipedia, http://en.wikipedia.org/wiki/Normal_distribution, accessed at June 2012.

28. *Wind Turbine Blade Analysis Using the Blade Element Momentum Method*. Version 1.0, Grant Ingram, December 13, 2005

29. Aydın C., *Analysis and Optimization of Monopile Type of Offshore Wind Turbines Under Wind and Wave Loading*, B. S. Thesis, Civil Engineering, Bogazici University, Istanbul, Turkey, 2011.

30. van der Tempel, J., *Design of Support Structures for Offshore Wind Turbine*, PHD Thesis, Delft Technical University, April 2006.

31. *Wind Turbine Model Figure*, Canadian Ministry of Agriculture, Food and Rural Affairs, http://www.omafra.gov.on.ca/english/engineer/facts/03-047.htm, accessed at September 2003.

32. Terzaghi K., *Evaluation of Coefficients of Subgrade Reaction,* Geotechnique 5, No. 4, pp. 297-326, 1955.

33. Das B. M., *Principles of Foundation Engineering - Seventh Edition*, Cengage Learning, 2011.

34. Chopra A. K., *Dynamics of Structures - Theory and Applications to Earthquake Engineering*, Prentice Hall, 1995.

35. van der Tempel, J., Molenaar, D.P. *Wind Turbine Structural Dynamics – A Review of the Principles for Modern Power Generation, Onshore and Offshore*, Wind Engineering, Vol. 26, No.4, pp. 211-220, 2002.

36. *Campbell Diagram*, Wikipedia, http://en.wikipedia.org/wiki/Campbell_diagram, accessed at July 2012.

37. American Petroleum Institute (API), *Recommended Practice for Planning, Designing and Constructing Fixed Offshore Platforms-Working Stress Design*, American Petroleum Institute, API RP-2A-WSD, 21st Edition 2000.

38. *Fatigue*, Wikipedia, http://en.wikipedia.org/wiki/Fatigue_(material), accessed at June 2012.

39. Jaap Schijve, *Fatigue of Structures and Materials-Second Edition*, Springer, 2009.

40. *Typical Stress Life (Wohler) Diagram*, University of Stavanger, http://www.ux.uis.no/~hirpa/KdB/ME/S-N%20diagram.pdf, accessed at May 2012.

41. Birkemoe, P.C., Srinivasan, R., *Fatigue of Bolted High Strength Structural Steel*, Journal of the Structural Division, Vol. 97, No. 3, pp. 935-950, USA, 1971.

42. Dowling, N. E., *Mechanical Behavior of Materials: Engineering Methods for Deformation, Fracture and Fatigue*, Prentice Hall, 1999.

43. Jonkman, J.M., Buhl, M.L., "*FAST User's Guide*", NREL/EL-500-38230, National Renewable Energy Laboratory, August 2005.